ARCHIWUM BUDOWY MASZYN

TOM XI 1964 ZESZYT 3

This research was supported by the Propulsion Division, AFOSR, SREP under Contract/Grant AF-AFOSR-129-64

A. K. OPPENHEIM, P. A. URTIEW and A. J. LADERMAN
University of California, Berkeley

VECTOR POLAR METHOD FOR THE EVALUATION OF WAVE INTERACTION PROCESSES

Abstract

Vector polar method is a graphical technique for the solution of wave interaction problems that are concerned with the overall results rather than with the progress of the process. The method is based on the use of wave polars, that is diagrams representing the loci of states attained by a given wave process in a coordinate system of which one component is pressure or velocity of sound and the other is particle velocity. Furthermore, if the ratio of pressures or sound speeds is represented on a logarithmic scale, usually as the ordinate, while the abscissa represents the change in particle velocity across the wave in a linear scale, then such a generalized hodograph plane has the property of a vector field, that is, the change of state brought about by the wave action is expressed in terms of a vector between the origin and any point of the polar. By simple vector addition one can then evaluate rapidly some quite complex wave interaction processes.

The utility of the method is illustrated here by a variety of shock-tube problems involving interactions between shocks, deflagrations, rarefaction waves, contact discontinuities and area change. Although the analysis of most of such problems is known, the application of the vector polar method led to the discovery of some interesting regimes of solutions that would be difficult to discern by the more laborious conventional techniques.

1. Introduction

One of the most useful ways of treating problems in non-steady gas dynamics is to consider them as results of wave interaction processes. A wave is a regime that propagates through the medium producing a change in state, subject to restrictions imposed by the principles of conservation of mass, species, momentum and energy. If, in particular, one wishes to know only what stationary states are created by a given wave interaction process without inquiring into the details of its progress, one should find the method introduced here particularly useful.

It is sufficient for this purpose to consider at first two elementary kinds of wave processes: one of the steady, or "Hugoniot-type", and the other non-steady, or „Riemann'ian". The first is distinguished by the fact that wave characteristics in the time-space domain (wave world-lines) are parallel, and includes the classical case of the gasdynamic discontinuity; the second is represented in its most elementary form by the simple, or uniform wave whose characteristics are straight lines.

Fundamental properties of these waves are derived here from basic principles, and the change of state brought about by their action is described in terms of polar diagrams which are then used for the vector polar method — a graphical technique for the evaluation of wave interaction processes. In order to treat wave interactions with area changes, the process of steady-state flow had to be also represented by means of suitable polar diagrams.

Foundations for the finite, wave interaction analysis were laid down by Riemann (1859), Hugoniot (1887—9) and Hadamard (1903). After some early attempts at a step-wise solution of some non-steady gasdynamic problems, such as those of Aschenbrenner (1937) and Pfriem (1941), the analysis has been reduced to an engineering reality by such contributions as those of Schultz-Grunow (1944), Sauer (1942), de Haller (1945), Jenny (1949) and many others who in the 1940's have popularized for this purpose the use of the method of characteristics. Since then such considerations became the nucleus of the rapidly expanding field of shock tube technology with publications too numerous to mention here. Most significant to the subject matter of this paper are the comprehensive texts of Courant and Friedrisch (1948), Rudinger (1955), Foa (1960), Glass and Hall (1958), Oswatitsch (1956), Von Mises (1958), Stanyukovich (1955), and Wright (1961), each containing quite an exhaustive bibliography. The importance to engineering practice of the non-steady flow phenomena that can be treated by our methods is demonstrated by the papers of Bannister and Mucklow (1948), Wallace and Mitchell (1952) and Mucklow and Wilson (1955).

The application of the method of characteristics to the solution of wave interaction processes is restricted in scope to the continuous domain of the phenomenon. The method can be therefore used only to trace the details of the process. In contrast to such an analysis "in the small", it is often of interest to know the results of the interaction without tracing the details of its progress, in other words to evaluate the stationary states and the wave system that has been attained by a given wave interaction after all the transient phenomena have died down. Moreover the answer to such a question yields information on the final bound to the solution of the inherently initial value problem of the hyperbolic domain treated by the method of characteristics.

It is for the purpose of getting such an answer directly that the vector polar methods is most suitable. In contrast to the method of characteristics, it provides only an analysis "in the large", leaving the zone of interaction completely outside the scope of inquiry. In many practical instances however this is quite sufficient, especially if the duration of the wave interaction event is short in comparison to the rest of the wave propagation processes under consideration. In our experience this was indeed true in the case of wave interaction phenomena that occur in the course of the development of detonation in gaseous mixtures [Oppenheim and Stern (1958), Oppenheim, Stern and Urtiew (1960)].

As one would suspect, there exists an equivalent method for the evaluation of steady-flow, two-dimensional wave interaction processes (see e..g Fallis et al (1953)); however its usefulness is handicapped by the awkwardness of polar dependence on initial Mach number and the inherent ambiguity associated with the possibility of a subsonic or a supersonic solution that can be obtained from the oblique shock polar for a given deflection angle.

With respect to non-steady flow, it is of interest to note that a method quite similar

to ours, but more restricted in scope, has been published independently in Poland by Kijkowski (1959).

For the sake of an orderly presentation the polars are here introduced first, and then their application to various wave interaction processes is illustrated by several examples. It should be noted however that the paper does not have to be read in the same sequence as it has been written. In fact, the reader may find it more amusing to acquaint himself first with solutions that may strike his interest, before learning about the derivation of the polars and their properties.

Notation

a — local velocity of sound,
A — velocity of sound ratio (a_y/a_x),
c_v — specific heat at constant volume,
e — internal energy,
h — enthalpy,
L — reference length,
M — Mach number,
p — pressure,
P — pressure ratio (p_y/p_x),
q — heat of reaction,
Q — non-dimensional heat of reaction $(q/p_x v_x)$,
R — area ratio,
t — time,
T — non-dimensional time coordinate $a_0 t/L$,
T — absolute temperature,
u — particle velocity,
U — non-dimensional particle velocity $[\Delta u/a_x = (u_y - u_x)/a_x]$,
$\bar{U}$ — non-dimensional particle velocity $(\Delta u/\sqrt{p_x v_x})$,
v — specific volume,
ν — specific volume ratio,
v — wave velocity relative to medium into which it propagates,
V — non-dimensional wave velocity (v/a_x),
$\bar{V}$ — non-dimensional wave velocity $(v/\sqrt{p_x v_x})$,
w — absolute wave velocity $(u + a)$,
W — non-dimensional absolute wave velocity $(U + A)$,
x — distance,
X — non-dimensional space coordinate (x/L),
γ — specific heat ratio,
ϱ — density.

Subscripts

a — refers to the initial velocity of sound,
c — denotes convergence,

d — denotes divergence,
i — denotes incident,
r — refers to reflected shock,
s — refers to a shock front (i.e. M_s its Mach number with respect to state into which it propagates, P_s pressure ratio across the wave),
o — refers to the initial state at rest,
x — refers to state immediately in front of wave or initial state for a process,
y — refers to state immediately behind the wave or final state for a process,
1, 2, 3... — denote states indicated on diagrams,
* — denotes critical value,
— denotes throat secti on.

2. Wave Polars

2.1. Steady Wave

A steady wave is one that propagates through space at a constant velocity without any distortion in its structure. Physically it is a plane wave whose world-lines (traces in space-time) are loci of constant states forming a family of straight parallel lines, as shown in Fig. 1. Notable examples of such waves are shocks, deflagrations and detonations.

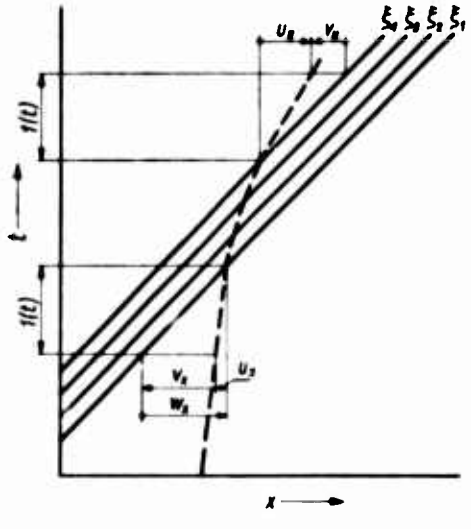

Fig. 1. Steady Wave in the Space-Time Domain

Basic wave relations, namely the expressions for the change in particle velocity that it produces, and for the velocity of its propagation, are obtained directly from the continuity and momentum equations which, with reference to Fig. 1, can be written respectively as follows:

$$\frac{v_x}{v_x} \Delta u = -\Delta v \tag{1}$$

and

$$\frac{v_x}{v_x}\Delta u = \Delta p \tag{2}$$

where $\Delta u = u_y - u_x$, $\Delta v = v_y - v_x$ and $\Delta p = p_y - p_x$.

The two relations are then obtained directly by multiplication and division, yielding:

$$(\Delta u)^2 = -\Delta p \cdot \Delta v \tag{3}$$

and

$$v_x^2 = -v_x^2 \frac{\Delta p}{\Delta v} \tag{4}$$

The appropriate Hugoniot equation for the wave process gives a functional dependence $\Delta p = f(\Delta v)$ with the use of which (3) and (4) become functions of a single variable, yielding the relation for the polar: $\Delta u = u(p)$ and for the propagation speed $v_x = v(p)$.

It should be noted that expressions (3) and (4) are walid irrespectively of the thermodynamic properties of the substance, and, within the dynamic meaning of p as the local normal component of the stress tensor and of v as the reciprocal of local density, they apply without invoking any principle of equilibrium. The most unambiguous non-dimensionalizing parameter for such a general case is the product $p_x v_x$ referred to the state of the medium into which the wave propagates. Introducing then $\bar{U} \equiv \Delta u/\sqrt{p_x v_x}$, $\bar{V} \equiv v_x/\sqrt{p_x v_x}$, $P \equiv p_y/p_x$ and $\mathcal{V} \equiv v_y/v_x$, equations (3) and (4) become:

$$U^2 = (P-1)(1-\mathcal{V}) \tag{3a}$$

$$\bar{V}^2 = (P-1)/(1-\mathcal{V}) \tag{4a}$$

For a perfect gas with constant specific heats the Hugoniot equation can be written as follows:

$$\frac{\gamma}{\gamma-1} pv - \frac{\gamma_x}{\gamma_x - 1} p_x v_x - q = \frac{p - p_x}{2}(v + v_x) \tag{5}$$

where q is the heat released per unit mass. With $Q \equiv q/p_x v_x$ it becomes:

$$\frac{\gamma+1}{\gamma-1} P\mathcal{V} - P + \mathcal{V} = 2Q + \frac{\gamma_x + 1}{\gamma_x - 1} \tag{5a}$$

which in terms of

$$\beta \equiv \frac{\gamma - 1}{\gamma + 1}$$

and

$$B \equiv (\gamma - 1)\left(Q + \frac{1}{\gamma_x - 1}\right) = \frac{\beta}{1-\beta}\left(2Q + \frac{1+\beta_x}{\beta_x}\right)$$

reduces to:

$$(P + \beta)(\mathcal{V} - \beta) = (B + \beta)(1 - \beta) \tag{5b}$$

demonstrating that the Hugoniot curve is a simple hyperbola with asymptotes $\mathcal{V} = \beta$ and $P = -\beta$.

Equations (3a) and (4a) yield now, with the use of equation (5b), the following expressions respectively for the wave polar and for the wave propagation velocity:

$$\bar{U}^2 = \frac{(P-1)(P-B)(1-\beta)}{(P+\beta)} \tag{6}$$

$$\bar{V}^2 = \frac{(P-1)(P+\beta)}{(P-B)(1-\beta)} \tag{7}$$

which summarize all the salient properties of these curves. For example, the condition of existence: $P > B$ if $P > 1$ which is evident from the form of (6) and (7) corresponds to the well known exclusion of the "forbidden zone" that is clearly delineated by (5b) as one implying that $P > B$ can be attained only if $\mathcal{V} < 1$.

It is customary for a perfect gas to express velocities in non-dimensional form by reference to the velocity of sound. Equations (6) and (7) give immediately the required expressions for the change in particle velocity:

$$U \equiv \frac{\Delta u}{a_x} = \frac{\bar{U}}{\sqrt{\gamma_x}} \tag{8}$$

and for the wave Mach number:

$$M \equiv \frac{v}{a_x} = \frac{\bar{V}}{\sqrt{\gamma_x}} \tag{9}$$

The ratio of the local velocities of sound is:

$$A \equiv \frac{a_y}{a_x} = \sqrt{\frac{\gamma_y}{\gamma_x} P\mathcal{V}} \tag{10}$$

or, with (5b):

$$A^2 = \frac{\gamma_y}{\gamma_x} P\left[\frac{(B+\beta)(1-\beta)}{(P+\beta)} + \beta\right] = \frac{\gamma_y}{\gamma_x} P \frac{\dfrac{2}{\gamma-1}B + P + 1}{\dfrac{\gamma+1}{\gamma-1}P + 1} \tag{10a}$$

If $\gamma_x = \gamma_y$ then $B = 1 + (\gamma-1)Q = 1 + \left(\dfrac{q}{c_v T_x}\right)$. For a shock wave $q = 0$, hence $B = 1$ and equation (6) [with equation (8)] becomes:

$$U^2 = \frac{2}{\gamma(\gamma+1)} \frac{(P-1)^2}{(P-1) + \dfrac{2\gamma}{\gamma+1}} \tag{11}$$

while equation (7) [with (9)] reduces to the well known relation between the Mach number and pressure ratio for a normal shock wave

$$P - 1 = \frac{2\gamma}{\gamma+1}(M^2 - 1) \tag{12}$$

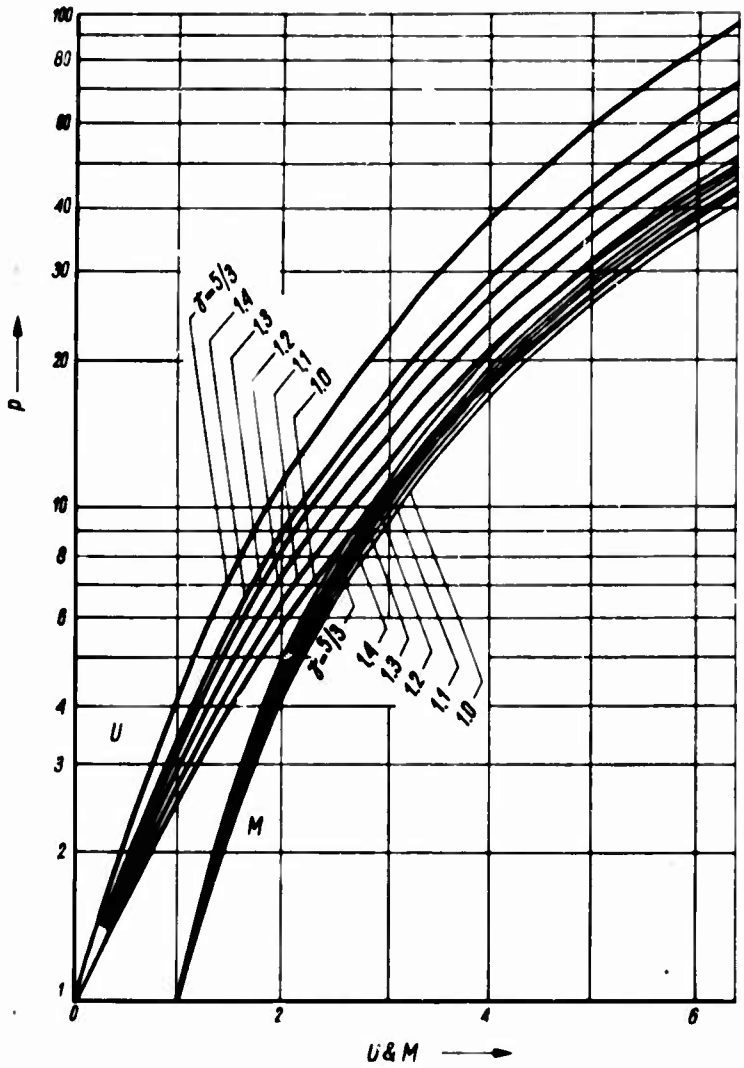

Fig. 2. Shock Polars for Perfect Gases in the Pressure Hodograph Plane and Shock Mach Numbers as a Function of Pressure Ratio

At the same time equation (10a) yields a simple relation:

$$A^2 = \frac{\beta P + 1}{P + \beta} P \tag{13}$$

Steady wave polars are introduced in Figs. 2 to 7. With a logarithmic scale for the pressure ratio and for the speed of sound ratio, while a linear scale is maintained for the velocity change across the wave, the polar diagrams are rendered a vectorial character. They form, in fact, generalized velocity hodographs, each polar representing a locus of end points of vectors starting from the origin whose one component is the change of particle velocity across a given wave $U \equiv \Delta u/a_x$ and the other is the logarithm of pressure ratio $P = p_y/p_x$ (or the sound speed ratio $A = a_y/a_x$).

Fig. 2 is a plot of equations (11) and (12) for various values of specific heat ratios, γ, from 1 to 5/3. Fig. 3 is a corresponding plot in the domain of the local velocity of sound.

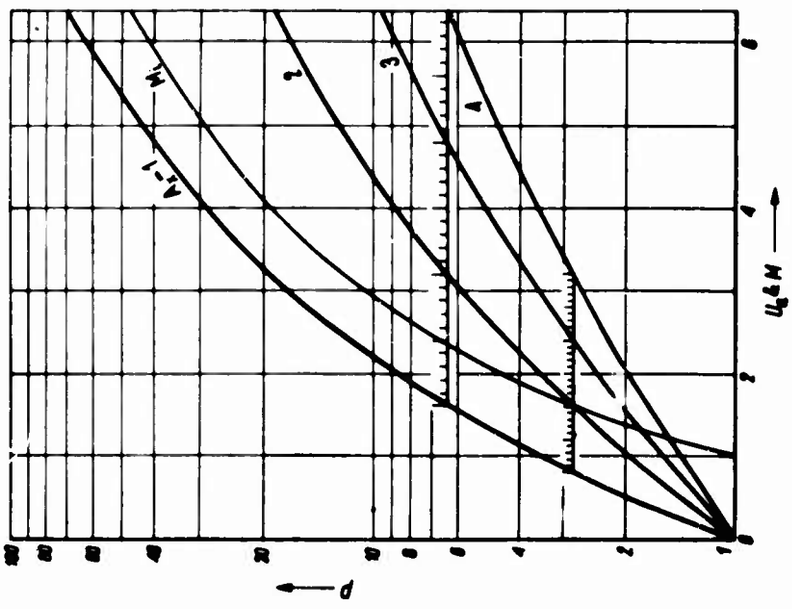

Fig. 4. Shock Polars and Mach Number for a Perfect Gas with $\gamma = 1.4$ in the Pressure Hodograph Plane

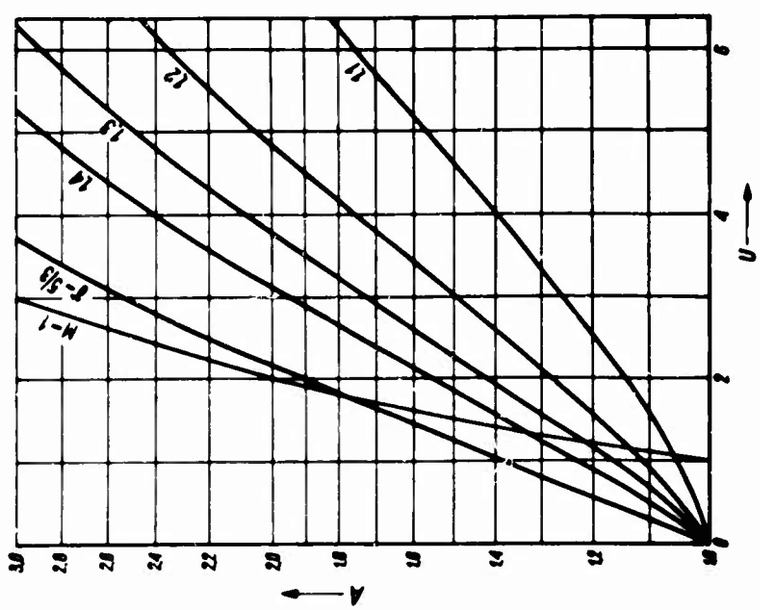

Fig. 3. Shock Polars for Perfect Gases in the Velocity of Sound Hodograph Plane

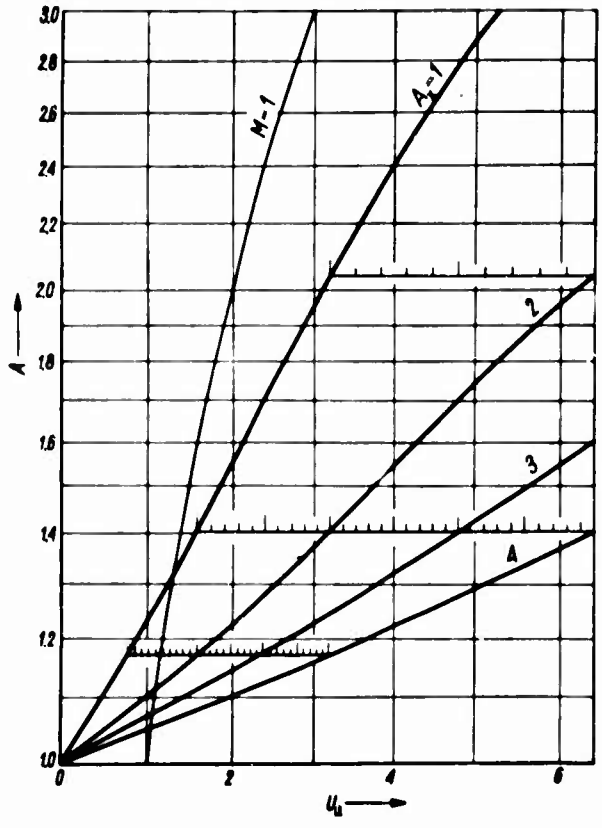

Fig. 5. Shock Polars for a Perfect Gas with $\gamma = 1.4$ in the Velocity of Sound Hodograph Plane

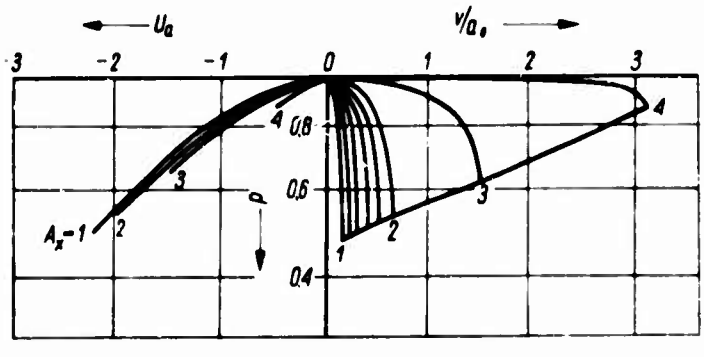

Fig. 6. Deflagration Polars and Mach Number for the Case od $\gamma_x = 1.4$, $\gamma_y = 1.2$ and $Q = 42.28$ (representing an $H_2 + 1/2\,O_2$ mixture) in the Pressure Hodograph Plane

The line of $M = 1$, which in Fig. 3 is simply a logarithmic curve, marks the limiting strength of shocks below which the flow, with respect to observer who is stationary in the regime into which the wave propagates, is subsonic, and above which it is supersonic.

Figs. 4 and 5 are the working diagrams for the solution of problems involving wave interaction processes. In this case the velocity change has to be related to some constant reference value of the velocity of sound which is usually taken as that of the undisturbed medium initially at rest. Consequently the abscissa in the working diagrams is $U_a \equiv \dfrac{\Delta u}{a_0} =$

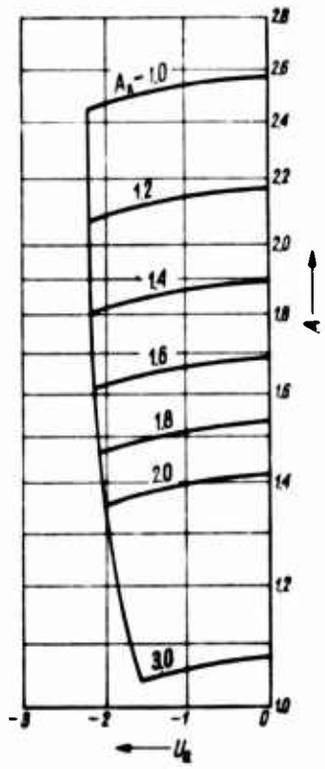

Fig. 7. Deflagration Polars for the Case of $\gamma_x = 1.4$, $\gamma_y = 1.2$ and $Q = 42.28$ in the Velocity of Sound Hodograph Plane

$= \frac{\Delta u}{a_x} \frac{a_x}{a_0} = UA_x$ and each polar becomes a function of the velocity of sound in the medium into which the wave propagates. Figs. 4 and 5 represent then such a family of polars derived quite simply from those of Figs. 2 and 3 for $\gamma = 1.4$ and A_x of 1, 2, 3, and 4 with interpolation scales for fractional values of A_x.

Figs. 6 and 7 represent working polar diagrams for a deflagration wave propagating to the right. The left hand side of Fig. 6 is essentially the plot of equation (6) [with (8)] the right hand side is the plot of equation (7) [with (9)] and Fig. 7 is transformed from Fig. 6 by the use of equation (10a). Under the assumption of perfect gas behavior of reactants and products, the deflagration is completely defined in terms of $\gamma_x = 1.4$, $\gamma_y = 1.2$, and $Q = 42.3$ that correspond here to the properties of a stoichiometric hydrogen-oxygen mixture, the value of heat release having been adjusted so that the polar curves would reproduce the experimental value of the Chapman-Jouguet detonation velocity.

2.2. Simple Wave

A simple wave is characterized by the fact that its world-lines are loci of constant states forming a family of straight (but not parallel) lines as shown in Fig. 4 which illustrates two intersecting simple waves. The regime of interaction is an example of an unsteady flow process that is outside the scope of our inquiry.

The two basic relations for the simple wave can be obtained by differentiation from those for a steady wave. Thus the process relation is from (1)

$$du = -a\frac{dv}{v} = a\frac{d\varrho}{\varrho} \tag{14}$$

or from (2)

$$du = \frac{vdp}{a}$$

while the expression for the local wave velocity is from (4);

$$a^2 = -v^2\frac{dp}{dv} = \frac{dp}{d\varrho} \tag{15}$$

Again the simplest non-dimensionalizing parameter is the local pv product so that (14) and (15) become:

$$\frac{du}{pv} = \frac{d(\log p)}{a} \tag{14a}$$

and

$$\frac{a^2}{pv} = -\frac{vdp}{pdv} \tag{15a}$$

In the integral form the process relation is, from (14):

$$\Delta u = \int_1^2 \frac{vdp}{a} \tag{16}$$

giving the generalized von Mises expression for the Riemann relation.

For an isentropic process the above becomes:

$$\Delta u = \int_1^2 \frac{dh}{a} \tag{17}$$

while (15a) yields:

$$\frac{a^2}{pv} = \frac{dh}{de} \equiv \frac{h}{e} + e\frac{d(h/e)}{de} \tag{18}$$

For a perfect gas, for which $\frac{d(h/e)}{de} = 0$, we obtain then the familiar expression

$$\frac{a^2}{pv} = \frac{h}{e} = \gamma \tag{19}$$

or

$$a^2 = \frac{pv}{e}h = (\gamma - 1)h$$

so that (17) reduces to

$$\Delta u = \int_1^2 \frac{2ada}{(\gamma - 1)a} = \frac{2}{\gamma - 1}\Delta a \tag{20}$$

The above is the well known Riemann invariance which in the present case represents the process relation for the wave.

The expression for the local velocity of wave propagation in terms of pressure is obtained directly from the isentropic relation for the ratio of local velocities of sound

$$A \equiv \frac{a_y}{a_x} = P^{\frac{\gamma-1}{2\gamma}} \tag{21}$$

The process relation (20) becomes then:

$$U \equiv \frac{\Delta u}{a_x} = \frac{2}{\gamma-1}(A-1) = \frac{2}{\gamma-1}(P^{\frac{\gamma-1}{2\gamma}}-1) \tag{22}$$

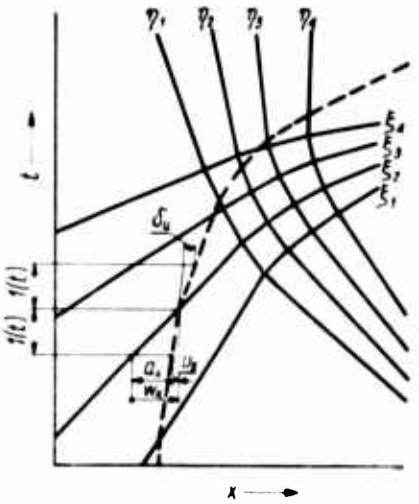

Fig. 8. Simple Waves in the Space-Time Domain

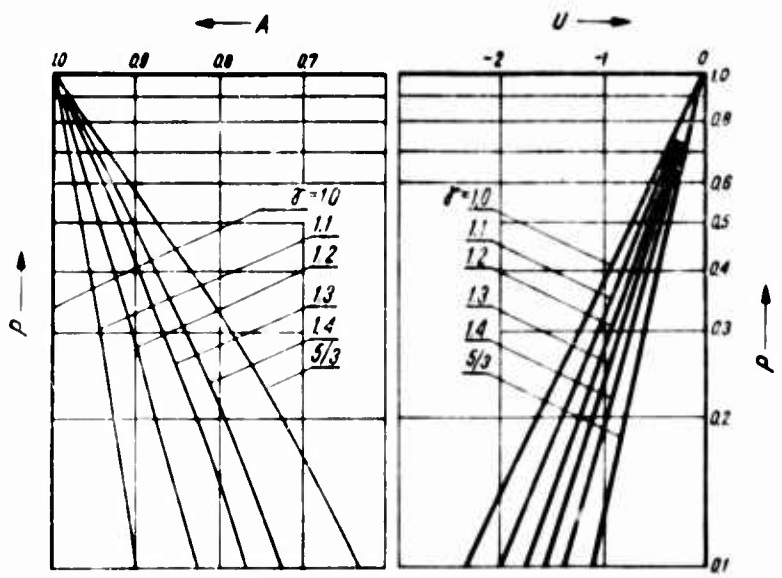

Fig. 9. Rarefaction Polars for Perfect Gases in the Pressure Hodograph Plane and Local Velocities of Sound as a Function of Pressure Ratio

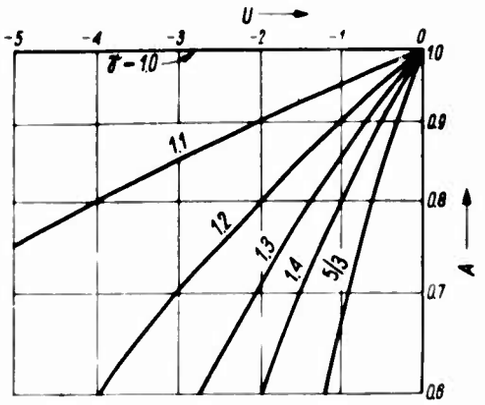

Fig. 10. Rarefaction Polars for Perfect Gases in the Velocity of Sound Hodograph Plane

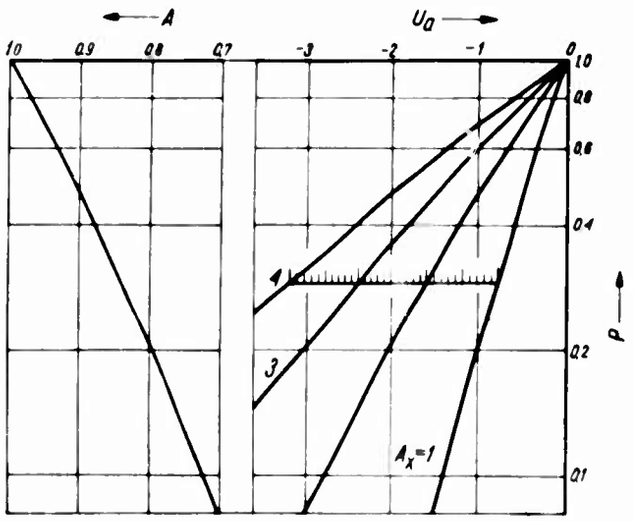

Fig. 11. Rarefaction Polars and the Velocity of Sound for a Perfect Gas with $\gamma = 1.4$ in the Pressure Hodograph Plane

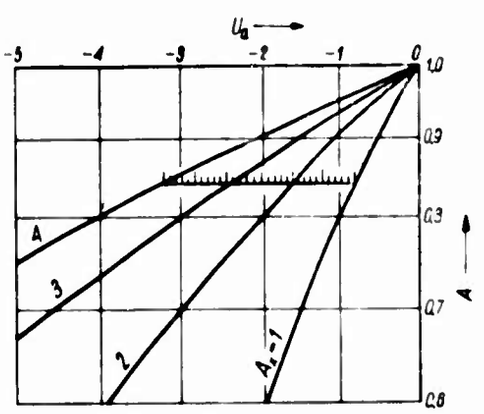

Fig. 12. Rarefaction Polars for a Perfect Gas with $\gamma = 1.4$ in the Velocity of Sound Hodograph Plan

Fig. 9 represents the plot of equation (21) on the left side, and that of equation (22) on the right side for a simple rarefaction wave propagating to the right. Fig. 10 is the corresponding polar diagram in the domain of the velocity of sound, representing essentially a cross-plot of the curves of Fig. 9. Similarly as in Figs. 2 and 3, the family of polars are given here in terms of the specific heat ratio as the parameter, covering the whole range of γ from 1 to 5/3.

Figs. 11 and 12 are working diagrams obtained from Figs. 9 and 10 for $\gamma = 1.4$ in exactly the same way as Figs. 4 and 5 were derived from Figs. 2 and 3.

2.3. Steady Flow Polars

In order to apply our graphical method to problems involving wave propagation through ducts with changes in cross-section area, the steady flow has to be specified in terms of polar diagrams as well. Such diagrams are represented in Figs. 13 to 16 for an isentropic flow of a perfect gas with $\gamma = 1.4$. The meaning of the polars is the same as

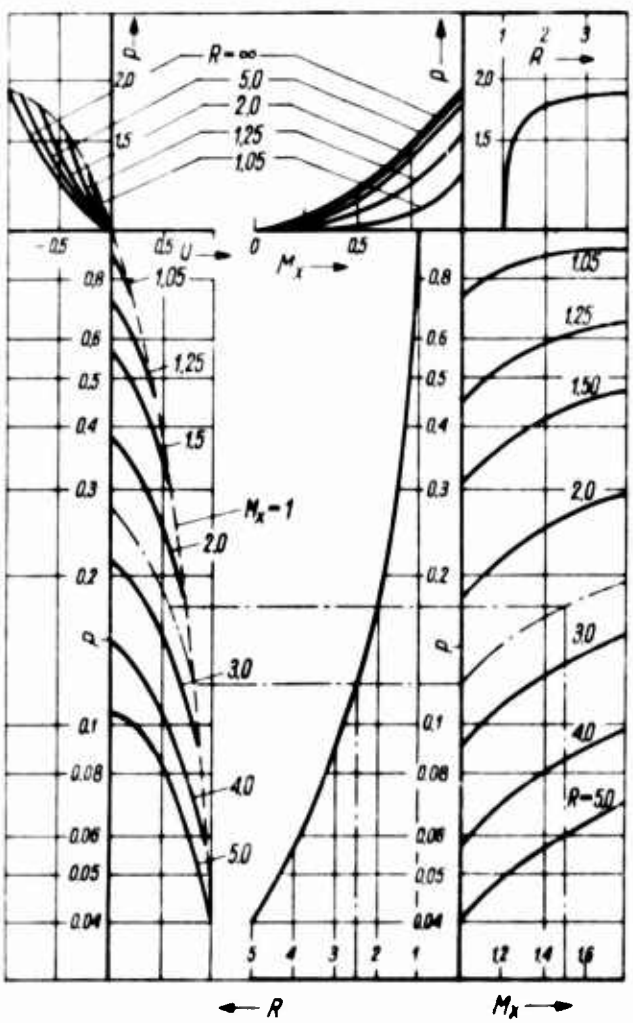

Fig. 13. Steady Flow Polars for Divergences in the Pressure Hodograph Plane ($\gamma = 1.4$)

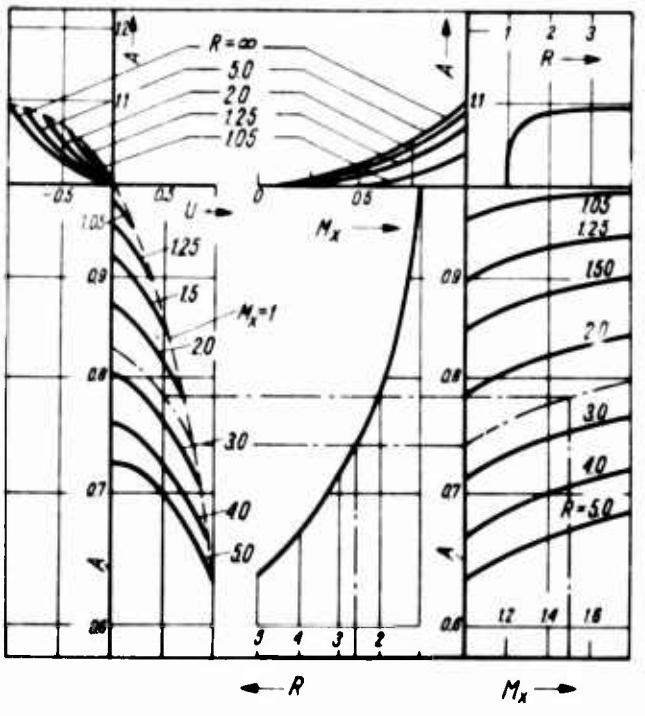

Fig. 14. Steady Flow Polars for Divergence in the Velocity of Sound Hodograph Plane ($\gamma = 1.4$)

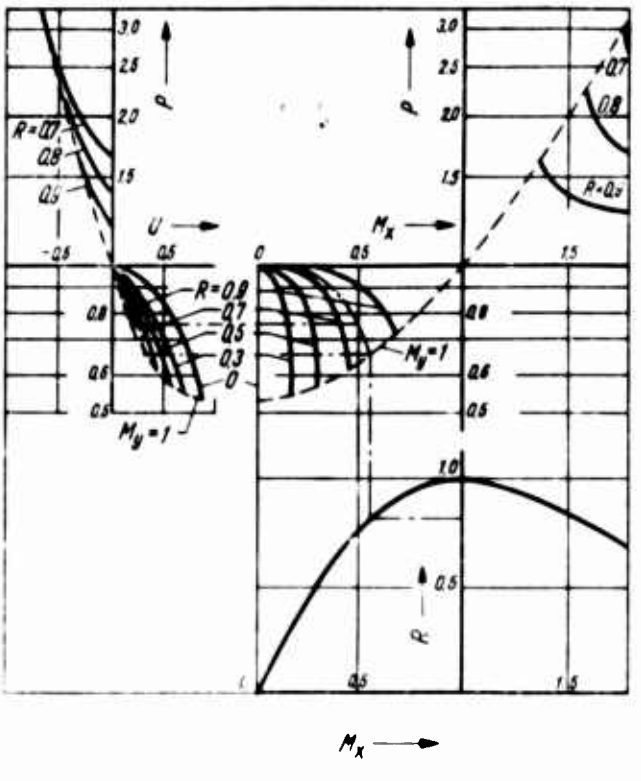

Fig. 15. Steady Flow Polars for Convergences in the Pressure Hodograph Plane ($\gamma = 1.4$)

before, that is they represent generalized velocity hodographs. The scales are identical, in order to permit vectorial superposition. However, unlike the non-steady polars, the end point of the steady flow velocity vector is not only subject to compatibility conditions between waves of the system resulting from a given interaction process, but it is also fixed by the value of the Mach number at the inlet. This, on one hand, gives rise to the generation of new waves, and on the other, necessitates the use of auxiliary graphs, which have been included on the right sides of Figs. 13 to 16.

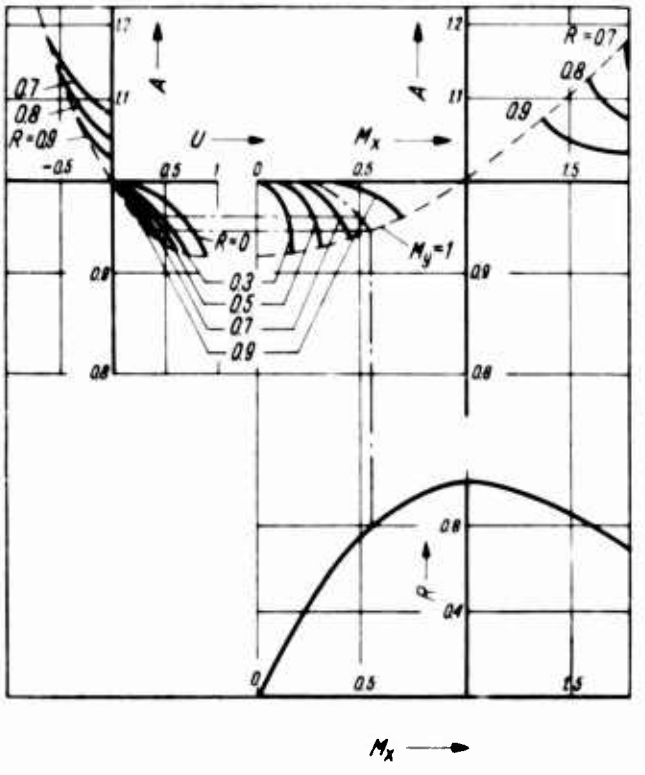

Fig. 16. Steady Flow Polars for Convergences in the Velocity of Sound Hodograph Plane ($\gamma = 1.4$)

The graphical procedure is illustrated by examples which, in Figs. 13 and 14, demonstrate how to obtain the end point of the steady flow vector for the area ratio $R = 2.5$, and the inlet Mach number, $M_i = 1.5$, while in Figs. 15 and 16 for the area ratio $R = 0.8$ and the inlet Mach number $M_i = 0.5$. As it is evident there, the area ratio is used first to locate the appropriate polar, and the Mach number at inlet specifies then the end point.

In terms of the pressure ratio the equation for the steady flow polar is:

$$U \equiv \frac{\Delta u}{a_x} = M\left[\frac{1}{R}\left(\frac{p_y}{p_x}\right)^{-\frac{1}{\gamma}} - 1\right] \tag{23}$$

and for the auxiliary curve:

$$M_x^2 \equiv \frac{1 - (p_y/p_x)^{\frac{\gamma-1}{\gamma}}}{\frac{\gamma-1}{2}\left[\frac{1}{R}(p_y/p_x)^{-\frac{2}{\gamma}} - 1\right]} \tag{24}$$

In terms of the velocity of sound ratio the corresponding equations are:

$$U \equiv \frac{\Delta u}{a_x} = M_x \left[\frac{1}{R} \left(\frac{a_y}{a_x} \right)^{-\frac{2}{\gamma-1}} - 1 \right] \tag{25}$$

and

$$M_x^2 = \frac{1 - \left(\frac{a_y}{a_x} \right)^2}{\frac{\gamma - 1}{2} \left[\frac{1}{R^2} \left(\frac{a_y}{a_x} \right)^{-\frac{4}{\gamma-1}} - 1 \right]} \tag{26}$$

The specific features of the steady flow polars will now be described for the subsonic and supersonic case respectively.

All subsonic polars pass through the origin of the coordinate system on the hodograph plane. On the other side all hodographs are limited by the condition of Mach number of unity obtained simply from equations (23) to (26) for $M_1 = 1$ which is represented in our diagrams by a broken line. For the divergence the limiting polar is that for $R = \infty$, corresponding to the case of an open end. The end point of this polar represents the state of vacuum attained at the section of infinite divergence, $M_y = 0$, for which the pressure ratio and the velocity of sound ratio at the end of the tube, acting now as the throat of the nozzle, attain their critical values $\left(\frac{\gamma+1}{2} \right)^{\frac{\gamma}{\gamma-1}}$ and $\left(\frac{\gamma+1}{2} \right)^{\frac{1}{2}}$ respectively, while the maximum change in particle velocity is $\frac{\Delta u}{a_1} = -1$. In the case of flow through a convergence the limiting polar is that corresponding to $R = 0$ and it represents the case of inflow from infinite reservoir while the coordinates of its end point are the critical values:

$$P_* = \left(\frac{2}{\gamma+1} \right)^{\frac{\gamma}{\gamma-1}}, \quad A_* = \left(\frac{2}{\gamma+1} \right)^{\frac{1}{2}} \text{ and } U_* = \left(\frac{2}{\gamma+1} \right)^{\frac{1}{2}}.$$

In contrast to the subsonic case, the supersonic polars have their singular points at the axis of ordinates $U = 0$, corresponding to the condition of $M_1 = \infty$. The position of each polar at this axis depends only on the value of the area ratio, namely:

$$\lim_{M_x \to \infty} P = R^{-\gamma} \tag{27}$$

and

$$\lim_{M_x \to \infty} A = R^{-\frac{\gamma-1}{2}} \tag{28}$$

which are obtained directly from equations (23) and (25) for $U = 0$ and $M_x = \infty$.

The choking condition for steady supersonic flow (i.e. $M_x = 1.0$ in the divergent case and $M_y = 1.0$ in the convergent case) is represented by the broken lines in Figs. 13–16. For the divergent case u approaches an asymptotic value, which in terms of the specific heat ratio is expressed as

$$\lim_{\substack{R\to\infty \\ M_y\to\infty}} U=\left(\frac{\gamma+1}{\gamma-1}\right)^{\frac{1}{2}}-1 \tag{29}$$

For $\gamma = 1.4$ this results in $\lim_{\substack{R\to\infty \\ M_y\to\infty}} U = 1.45$. Asymptotic values for other specific heat ratios are listed in Table 1. The choking line in the convergent case has no asymptote since both U and P go to infinity.

Table 1
Functions of Specific Heat Ratio

Quantity	Equation	Ratio of Specific Heats, γ					
		1.0	1.1	1.2	1.3	1.4	5/3
$\lim_{\substack{R\to\infty \\ M_y\to\infty}} U$	29	∞	3.58	2.32	1.77	1.45	1.00
$M_\bullet$	39	1.619	1.697	1.797	1.918	2.069	2.757
$\lim_{R\to\infty} M_i$	38	1.0	1.09	1.125	1.145	1.151	1.17
$\lim_{M_i\to\infty} R_{III}$	46	0	0.008	0.13	0.375	0.648	0.933
$\lim_{M_i\to\infty} R_{IV}$	47	0	0.516	0.68	0.772	0.838	0.957
$\lim_{R\to\infty} M_i$	—	1.271	1.37	1.47	1.58	1.719	2.075
$\lim_{M_i\to\infty} R_{III}$	57	∞	12.5	7.7	2.67	1.543	1.072
$P_\bullet$	60	2.62	7.28	8.7	9.43	10.35	12.75
$\lim_{M\to\infty} (P_4)_{IV}$	65	2.615	4.7	5.12	5.54	5.96	7.16

3. Examples

The vector polar methods is illustrated here by the following elementary exaples: the shock tube problem, the interaction between a shock wave and a deflagration front, the merging of shocks and the merging of a rarefaction wave with a shock front.

3.1. The Shock Tube Problem

The simplest case of wave interaction is that of the start of a simple shock tube. Before the interaction there are two regimes, both at rest, each at a different pressure, separated by a diaphragm. The diaphragm is suddenly removed, causing a shock to move into the low pressure and a rarefaction front into the high pressure regime.

In the example of Fig. 17 the initial diaphragm pressure ratio was $P_4 = 2.62$. The medium on both sides of the diaphragm was kept at the same initial temperature, and it was assumed to behave essentially as a perfect gas with $\gamma = 1.4$. With reference to the solution depicted on Fig. 17 the fact that there is a shock propagating into the regime at state 0 is reflected on the hodograph plane by the shock polar for $A_x = 1$ of Fig. 6 starting from point $U = 0$, $P = 1$ and $A = 1$. At the same time the fact that a rarefaction

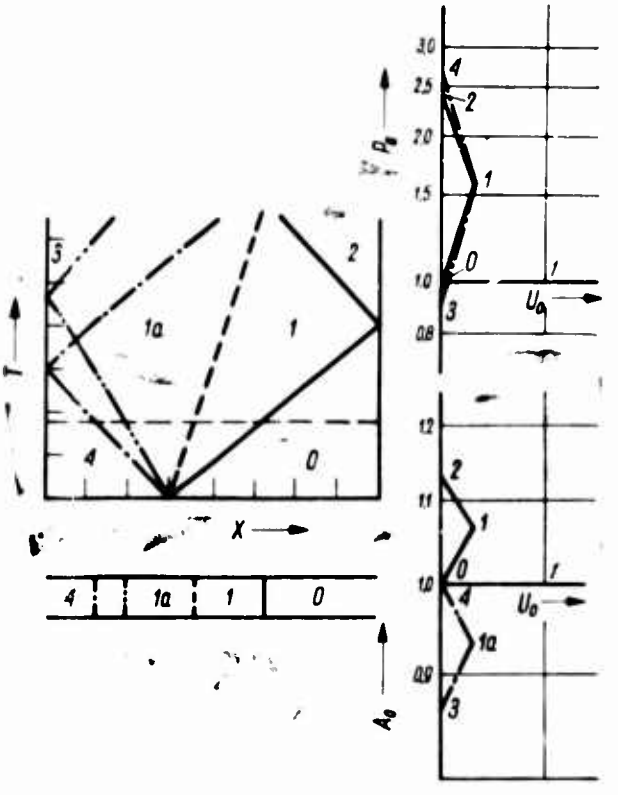

Fig. 17. Simple Shock Tube Problem

is moving into state 4 is represented on the hodograph plane by the rarefaction polar for $A_x = 1$ of Fig. 11 starting from point $U = 0$, $P = 2.62$ and $A = 1$. The intersection of the two polars on the plane determines states (1, 1a) while the corresponding points in the $A - U$ plane specify the conditions on the two sides of the contact discontinuity as shown in Fig. 17 and in Table 2. Included there moreover is the reflection of the shock wave from the closed end, establishing state 2, and the reflection of the rarefaction fan from the other side producing state 3. These two states are determined directly by the intersection with the $U = 0$ axis of a shock polar starting from state 1 for $A_1 = 1.067$, and of a rarefaction wave starting from state 1a for $A_{1a} = .933$.

The above problem is indeed so simple that for a perfect gas with constant specific heats one can solve it algebraically without any difficulty. In fact, according to equation (11) the particle velocity behind the shock is given by:

$$U_1^2 = \frac{2}{\gamma(\gamma+1)} \frac{(P_1 - 1)^2}{(P_1 - 1) + \dfrac{2\gamma}{\gamma + 1}} \tag{30}$$

while behind the rarefaction wave equation (22) gives

$$\frac{u_{1a}}{a_4} = \frac{2}{\gamma - 1}\left[1 - \left(\frac{p_{1a}}{p_4}\right)^{\frac{\gamma-1}{2\gamma}}\right] \tag{31}$$

Since $u_1 = u_{1a}$ and $p_1 = p_{1a}$ one obtains then directly:

$$\frac{2a_4}{\gamma - 1}\left[1 - \left(\frac{p_1}{p_4}\right)^{\frac{\gamma-1}{2\gamma}}\right] = \sqrt{\frac{2}{\gamma(\gamma+1)}}\frac{(P_1 - 1)a_0}{\sqrt{(P_1 - 1) + \frac{2\gamma}{\gamma+1}}} \tag{32}$$

whence:

$$P_4 = P_1\left\{1 - \frac{(\gamma-1)(P_1-1)}{\sqrt{2\gamma(\gamma+1)A_4}\left[(P-1) + \frac{2\gamma}{\gamma+1}\right]^{1/2}}\right\}^{-\frac{2\gamma}{\gamma-1}} \tag{33}$$

Equation (26) yields the diaphragm pressure ratio, P_4, that is required to produce a given shock pressure ratio, P_1, which is related in turn to the incident shock Mach number by equation (12).

Similarly, it can be shown that as a consequence of the requirement that particle velocity at the closed end of the tube must be zero behind the reflected shock wave,

$$p_2 = p_1\frac{(2\beta+1)P_1 - \beta}{\beta P_1 + 1} = p_1\frac{\frac{3\gamma-1}{\gamma-1}P_1 - 1}{P_1 + \frac{\gamma+1}{\gamma-1}} \tag{34}$$

yielding a straight forward expression for the pressure attained behind the reflected wave in terms of a given pressure ratio of the incident shock.

It should be noted that the algebraic solution follows in essence the graphical treatment. The latter moreover has the advantage of simplicity and generality since, as contrasted to the former, it can be applied as easily to the inverse as to the direct problem, and it is not restricted in scope to any particular form of the equation of state.

3.2. Interaction Between a Shock and a Deflagration Wave

Consider a head-on collision between a shock moving to the right at $M_s = 1.6$ and a deflagration moving to the left with $M = 0.14$. As shown in Table 2 the shock raises the pressure by a factor of 2.75 while the deflagration is associated with a pressure drop of 40%. The results of the interaction in terms of stationary states that should be attained provided that the deflagration survives the shock impact are shown in Fig. 18. As it appears there the transmitted deflagration polar reaches the Chapman-Jouguet state (2) before intersecting the polar (10–20) of the transmited shock. The only way then that a compatible wave system would be obtained is by postulating that the interaction is associated with the generation of a rarefaction wave (2–20) that propagates immediately behind the Chapman-Jouguet state.

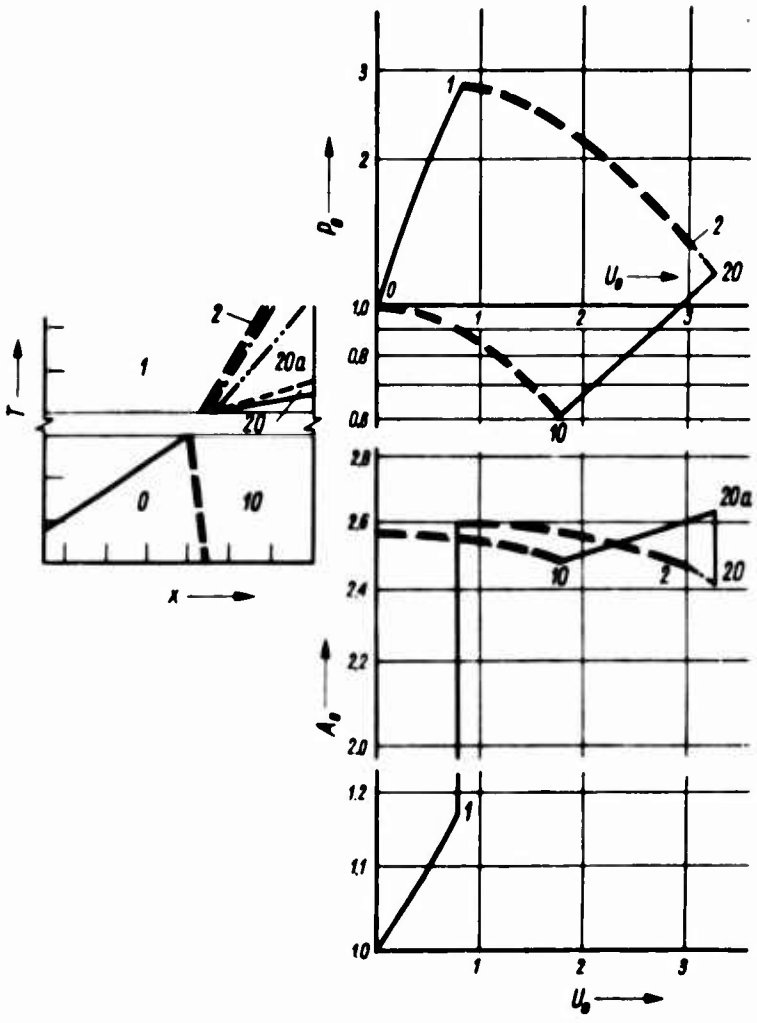

Fig. 18. Interaction between a Shock and a Deflagration Wave

The graphical technique suggests here directly the appearance of the rarefaction wave whose existence could not have been so easily deduced by analysis.

3.3. Shock Merging

Two shocks propagating in the same direction must merge and, as it has been proven by von Neumann (1943), such an interaction results in a transmitted shock and a reflected rarefaction. As illustrated in Fig. 19, the appearance of the rarefaction wave is a consequence of the fact that, for shocks propagating to the right, the pressure velocity hodograph has a property that a shock polar started from any point of another shock polar must lie to the left of it. Consequently, the only way to attain a compatible wave system is by postulating the existence of a rarefaction such as 2—3 in Fig. 19. It is of interest to note that the opposite holds true for the sound speed velocity hodograph, so that state 2 has a lower sound speed than state 3. Numerical results of our graphical solution are again presented in Table 2.

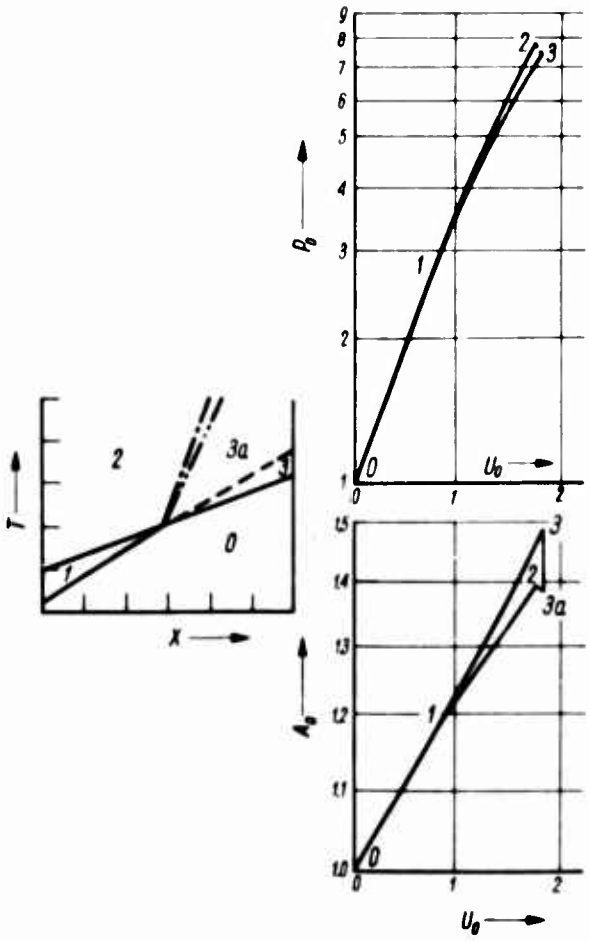

Fig. 19. Shock Merging

These interesting properties of the hodographs reflect essentially the fact that, in order to attain a given particle velocity, higher pressure has to be reached by an isentropic compression wave (equivalent to an infinite number of shocks, each propagating into a regime produced by the preceding one) rather than by a shock wave. In contrast to this, the sound speed (or temperature) attained by the isentropic pressure wave is lower than that produced by the shock which produces the same particle velocity.

3.4. Merging of a Rarefaction Wave with a Shock

The various wave systems that can be obtained by a rarefaction wave merging with a shock have been described by Glass and Hall (1958). A simple graphic l interpretation of these results is given in Fig. 20 which illustrates the case of a rarefaction moving to the right and merging with a shock wave that propagates ahead of it. Referring to the pressure velocity hodograph, it appears that a rarefaction started from any point of the shock polar of the same family has, on one hand, a larger initial slope than the polar but, on the other, it is straighter than the polar and, consequently, there must exist another intersection such as point 2′4′ in Fig. 20. Above this state, the interaction results in a re-

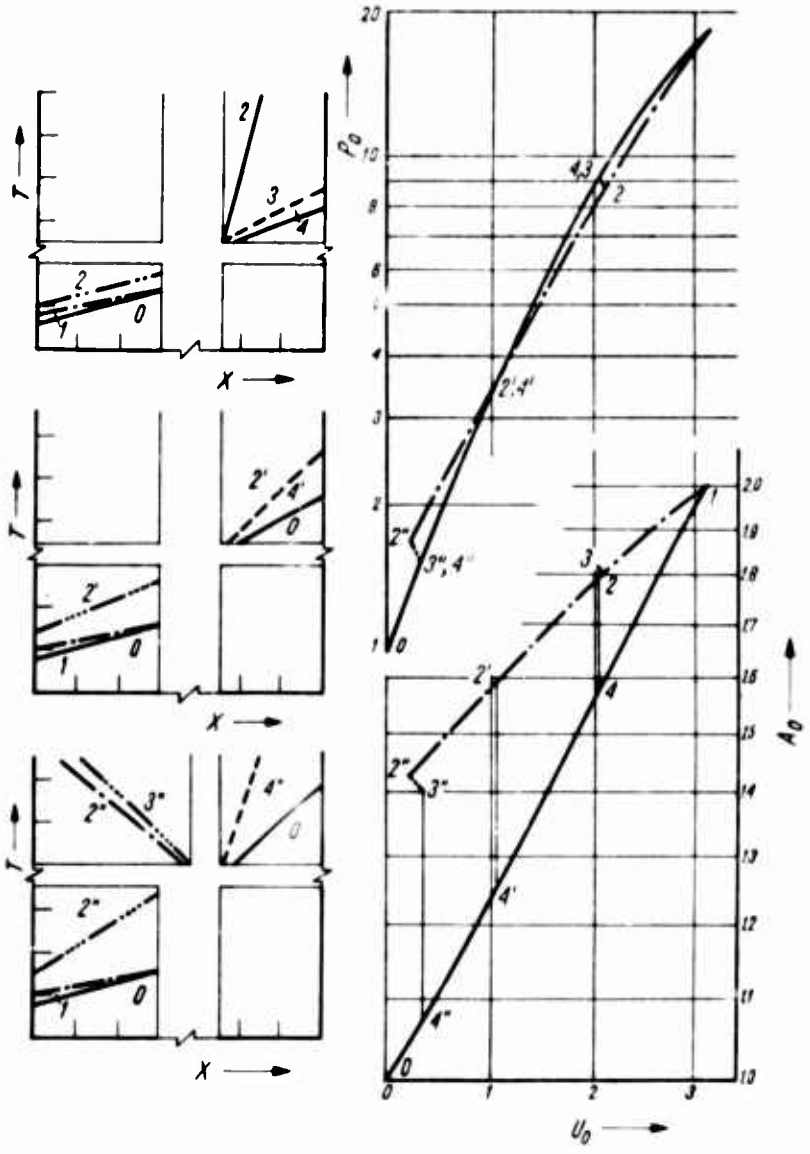

Fig. 20. Merging of a Rarefaction Wave with a Shock

flected shock, below it, in a reflected rarefaction, while state 2′4′ corresponds to the case where there is only a transmitted shock and, except for the contact discontinuity, there is no reflected wave. As before, numerical results of the solutions are listed in Table 2.

4. Interactions Between, Shocks and Area Changes

Of fundamental importance to shock tube technology is the interaction between a plane shock front and a section in the tube where an area change takes place. Basically, it is an extension of the classical problem concerned with the effect that the change in cross-section area has on the propagation of sound waves in tubes. The greatest impetus to the study of this problem with respect to finite amplitude shock fronts was derived from the application of shock tubes as drivers for hypersonic wind tunnels which involves the interaction between the shock and the divergent inlet to the test section. The general

interest, however, into the fundamental features of the interactions between finite amplitude waves and channels of varying area led to a number of investigations which included other types of area change, such as convergences in the tube cross-section, as well as obstacles made mostly of grids and wire gauzes.

The main conclusion derived from these studies is the realization that most of the experimental results check very well with one-dimensional analysis for a perfect gas with constant specific heats. Each paper was concerned only with a certain specific aspect of the subject of shock interactions with area changes and, consequently, the coverage of this field has been so far quite sporadic.

The facility afforded by the vector polar method permits us to attain a comprehensive view upon the whole subject of such interactions. The field is covered by the consideration of the interactions of shocks with, first, divergences, then convergences in the tube cross-section area and, finally, with convergent-divergent nozzles. In the particular case of equal exit and inlet, the latter represents also an idealization of the case of an obstacle, such as a grid, affecting the whole cross-section, that is inserted in a constant area duct.

4.1. Interaction with Area Divergence

All the cases of various plane wave systems that can result from an interaction between a shock and an area divergence in a tube are represented in Fig. 21. Numerical results for these problems are listed in Table 2. Each contains the traces of the various wave fronts plotted to scale in the non-dimensional time-space plane whose coordinates are: $X = \frac{x}{L}$ and $T = \frac{a_0 t}{L}$ where x is the space coordinate, t is the time, L is the reference length, and a_0 is the velocity of sound in the undisturbed medium which initially is at rest. Shown underneath each wave diagram is a cut through the wave system taken at a suitable time instant. On the right are the graphical solutions obtained by the use of the vector polar method in the $P-U$ and the $A-U$ planes for a perfect gas with a specific heat ratio $\gamma = 1.40$.

Cases 1 through 4 of Fig. 21 correspond to the same Mach number $M_i = 1.7$ of the incident shock. The first refers to a very small divergence of an area ratio $R = 1.03$. The interaction under such circumstances produces eventually a rarefaction wave traveling upstream and a transmitted shock which, as in all the other cases involving divergences, is weaker than the incident shock.

As the area ratio is increased, the trailing edge of the rarefaction fan is "pushed back" until it becomes stationary at the inlet to the divergence. Thereupon, the interaction produces a standing shock at some intermediate cross-section. Such a situation is illustrated by Case 2, which corresponds to an area ratio $R = 1.08$, only a few percent larger than that of Case 1.

When the area ratio is increased still more, the standing shock wave is "pushed back" until it finally becomes swept downstream out of the divergence producing the typical configuration of hypersonic shock tunnels. This is shown as Case 3 corresponding to an area ratio $R = 1.25$.

Reasoning "by extrapolation" one would expect at this point that, as the area ratio is increased still more, the amount by which the shock is swept back would also increase

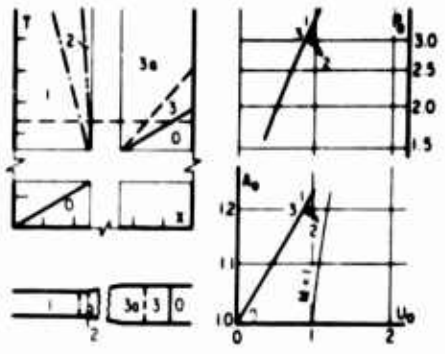

1

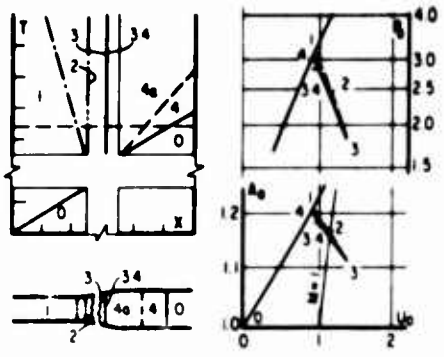

2

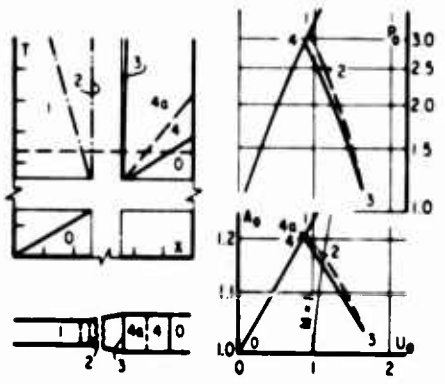

3

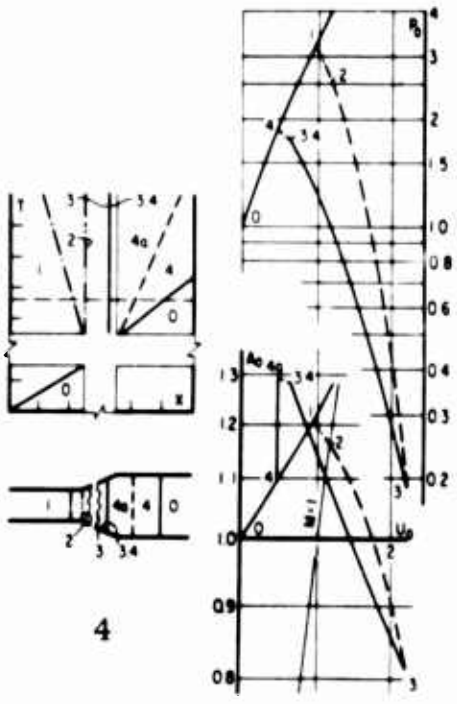

4

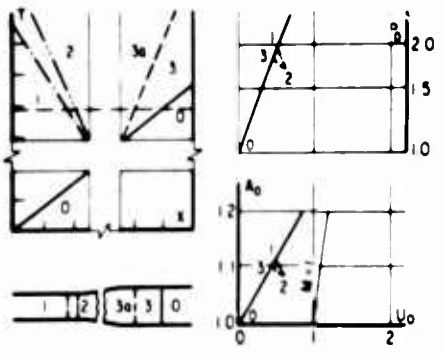

5

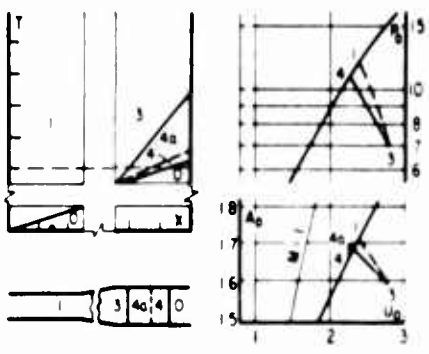

6

Fig. 21. Shock Interactions with Area Divergences

1. $M_i = 1.70$: $R = 1.03$ 2. $M_i = 1.70$: $R = 1.08$ 3. $M_i = 1.70$: $R = 1.25$
4. $M_i = 1.70$: $R = 4.45$ 5. $M_i = 1.34$: $R = 1.25$ 6. $M_i = 3.20$: $R = 1.25$

indefinitely. But this is not the case. It turns out that the amount of sweepback has an upper bound so that, after reaching a maximum, it decreases until, with sufficiently large divergences, the shock becomes again stabilized inside it. A wave pattern obtained then is demonstrated by Case 4 which corresponds to an area ratio $R = 4.45$.

In order to complete the survey of the various conditions obtainable as a result of the interaction between a plane shock and area divergence, two more solutions are shown in Fig. 21 for the same area ratio $R = 1.25$ as that of Case 3, but for different strengths of the incident shock. In Case 5 the incident shock Mach number is $M_i = 1.34$, while Case 6 corresponds to $M_i = 3.2$. Conspicuous in the latter is the absence of the rarefaction fan propagating upstream — a characteristic feature of all cases when the Mach number of the incident shock is high enough to produce supersonic flow in the tube. For a perfect gas with $\gamma = 1.4$, such a limiting value of the Mach number is $M_i^* = 2.069$. Values of such critical Mach number for other specific heat ratios are given in Table I.

4.2. Interactions with Area Convergences

In the case of shock impingement on an area convergence in a tube there is an interesting peculiarity in that there exists a regime where three different solutions satisfy the compatibility condition at the same time. They correspond to the cases of a reflected

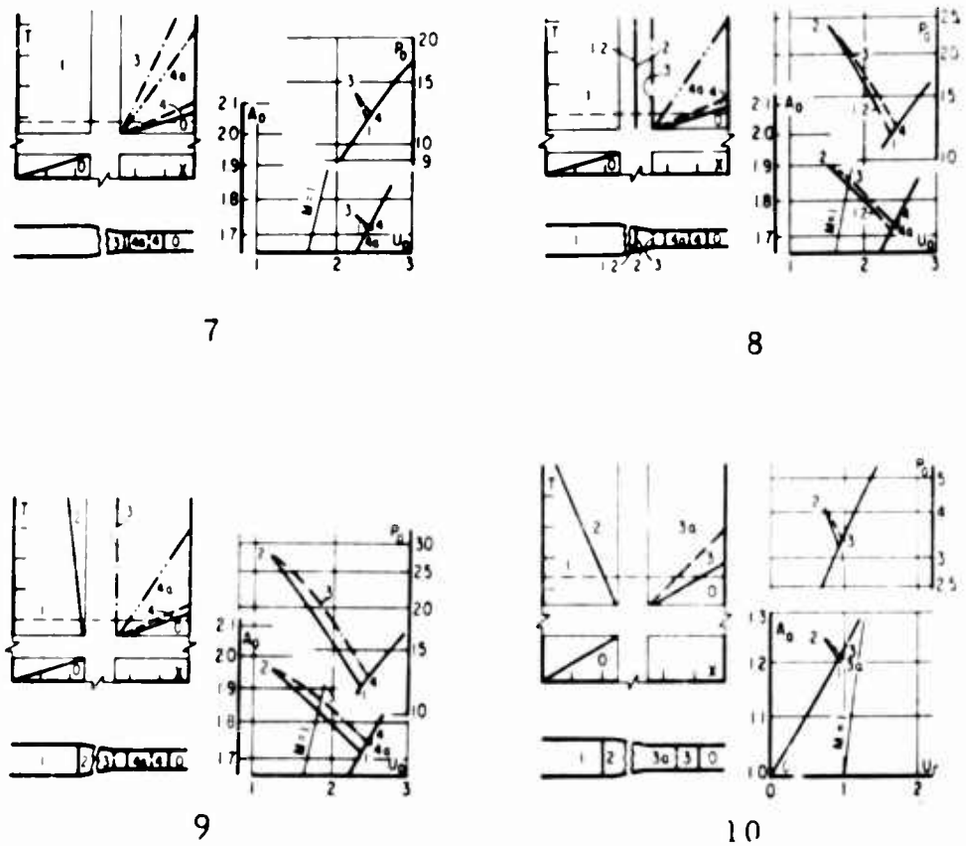

Fig. 22. Shock Interactions with Area Convergences

7. $M_i = 3.20$; $R = 0.95$ 8. $M_i = 3.20$; $R = 0.84$
9. $M_i = 3.20$; $R = 0.84$ 10. $M_i = 1.34$; $R = 0.84$

shock, a standing shock and a transmitted shock without reflection. This was the subject of one of our earlier papers (Oppenheim, et al. (1959)) which has been followed by a number of publications that were concerned with a more detailed analysis of this phenomenon, namely those of Rudinger (1960) Brower (1961) and Ciolkowski (1961). Moreover it turned out that our observation about the possibilty of establishing more than one wave pattern as a result of shock interaction with a converging duct received independently an experimental verification (Bird 1959).

For the sake of completeness, three other representative cases, each for a different area ratio but all corresponding to the incident shock Mach number, $M_i = 3.2$, of the last example of Fig. 21, are shown in Fig. 22. The first (Case 7) for $R = 0.95$, represents an interaction without reflection, the second (Case 8) for $R = 0.91$ illustrates the attainment of a standing shock, and the third (Case 9) for $R = 0.84$, demonstrates an interaction producing a reflected shock. With reference to the latter, as the Mach number of the incident shock is decreased, the strength of the rarefaction fan, 3—4a, becomes weaker until it disappears altogether. This is demonstrated as Case 10 corresponding to the same area ratio, $R = 0.84$ as Case 9 but to a different incident shock Mach number, namely $M_i = 1.70$, i.e. the same as that used for Cases 1 to 4. Again numerical results of the solution are listed in Table 2.

4.3. Summary of Shock Interactions with Single Area Changes

As it is apparent from the preceding discussion, the question as to what kind of a wave system results from a given interaction depends only on the Mach number of the incident shock and on the area ratio that specifies the geometry of the system.

This is summarized in Fig. 23 where all the various regimes of solutions are given in terms of the area ratio and the Mach number of the incident shock for a perfect gas with a constant specific heat ratio, $\gamma = 1.40$. The conditions of the various examples of Figs. 21 and 22 are indicated in Fig. 23 by points numbered correspondingly to the cases which they represent.

By reference to Fig. 23 one can quickly ascertain what kind of a wave pattern can be eventually produced by a given interaction. Each wave system occupies a regime in the M_i R plane. The boundaries have been determined analytically and their properties are described in Appendix I.

Fig. 23 can be generalized easily to other values of the specific heat ratio, γ if the effect of this parameter on its characteristic points are known. Such information is given in Fig. 24 where asymptotes for lines III (Lim R_{III}), IV (Lim R_{IV}), I (Lim M_I), and V (Lim M_V) are expressed in terms of γ. All these lines stem from a point on the $R = 1$ axis representing the state when the flow immediately behind the incident shock becomes sonic in the tube; consequently the dependence on γ of the Mach number of such shocks, M_*, is also included there.

Since the shape of the lines remains essentially the same, they can be drawn for any value of γ on the basis of the information provided by Fig. 24. In order to describe the extent by which γ can influence the boundaries, curves of Fig. 23 are redrawn in Fig. 25, for two extreme values of this parameter, namely 1.0 and 5/3. It is of interest to note that for convergences the regime of "peculiarity" decreases quite rapidly as γ becomes larger.

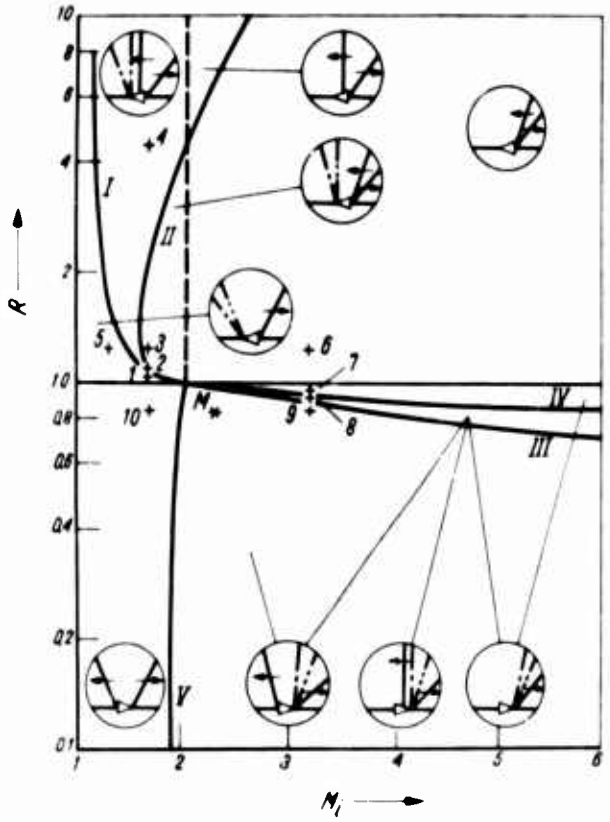

Fig. 23. Regimes of Solutions for Shock Interactions with Single Area Changes in the Mach Number-Area Ratio Plane ($\gamma = 1.4$)

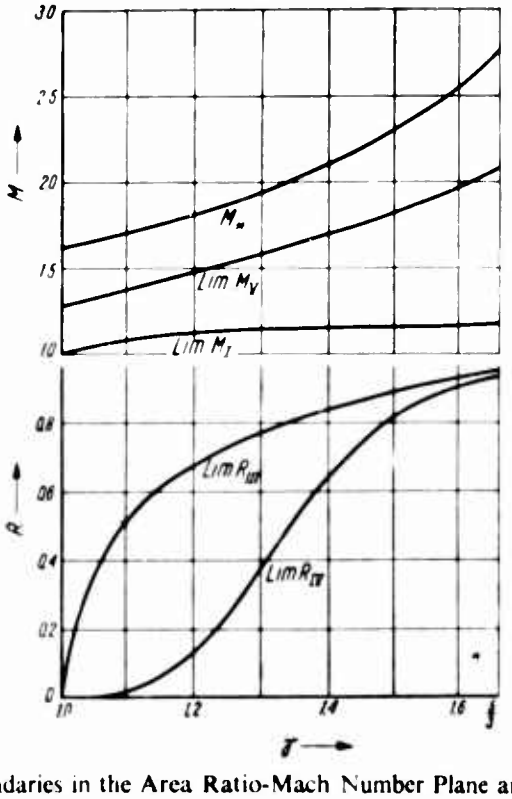

Fig. 24. Asymptotes of Boundaries in the Area Ratio-Mach Number Plane and the Critical Shock Mach Number as a Function of Specific Heat Ratio

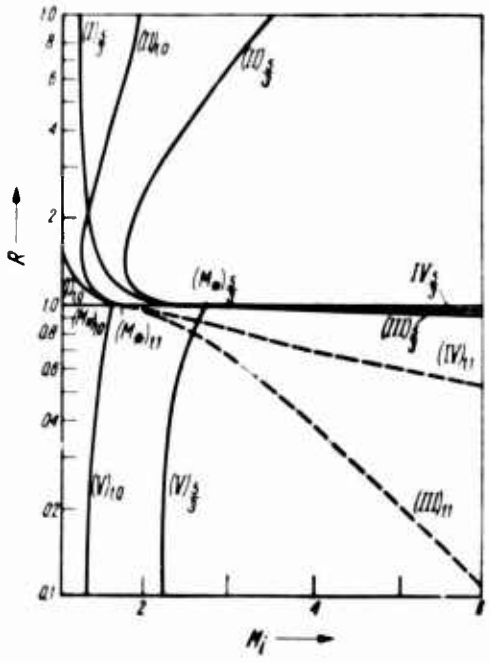

Fig. 25. Effect of Specific Heat Ratio on the Mach Number-Area Ratio Plane, Fig. 23.

4.4. Interactions with Convergent-Divergent Nozzles

Several solutions of shock interactions with convergent-divergent nozzles are presented in Fig. 26 and tabulated in Table 2.

The first two refer to the same nozzle whose geometry is fixed by area ratios $R_i/R_d = 0.444/1.666$, under the influence of different incident shock Mach numbers $M_i = 1.76$ and $M_i = 2.581$ respectively, the former generating a subsonic and the latter a supersonic flow through the duct. The resulting wave system of Case 1 resembles the left side of Case 9 in Fig. 22 and the right side of Case 3 in Fig. 21, while Case 2 in Fig. 26 is a combination of the left side of Case 10 in Fig. 22 and of the right side of Case 6 in Fig. 21.

The rest of solutions in Fig. 26 refer to experiments actually reported in the literature. Cases 3 and 4 correspond to conditions produced by a 30 mesh grid of 38% porosity taht has been used by Franks (1957) in a shock tube with incident shock Mach numbers $M_i = 1.649$ and 2.30 respectively. Cases 5 and 6 are those of experiments performed by Dosanjh (1955) who used a grid with a solidity of 25% with incident shock Mach numbers of $M_i = 1.58$ and 2.30.

The results are summarized in Table 3 which demonstrates that, in addition to its simplicity and universality, the vector polar methods offers a sufficiently good accuracy for all practical purposes.

Similarly as for single area changes, all solutions for nozzles can be summarized in a single M_i—R plot, as shown in Fig. 27 for $\gamma = 1.40$. If the flow through the convergent section of the nozzle is wholly subsonic, the resulting flow system can be calculated, disregarding completely the geometry of the nozzle and substituting for it only a single area change that is specified by the overall ratio of the exit to inlet cross-section area.

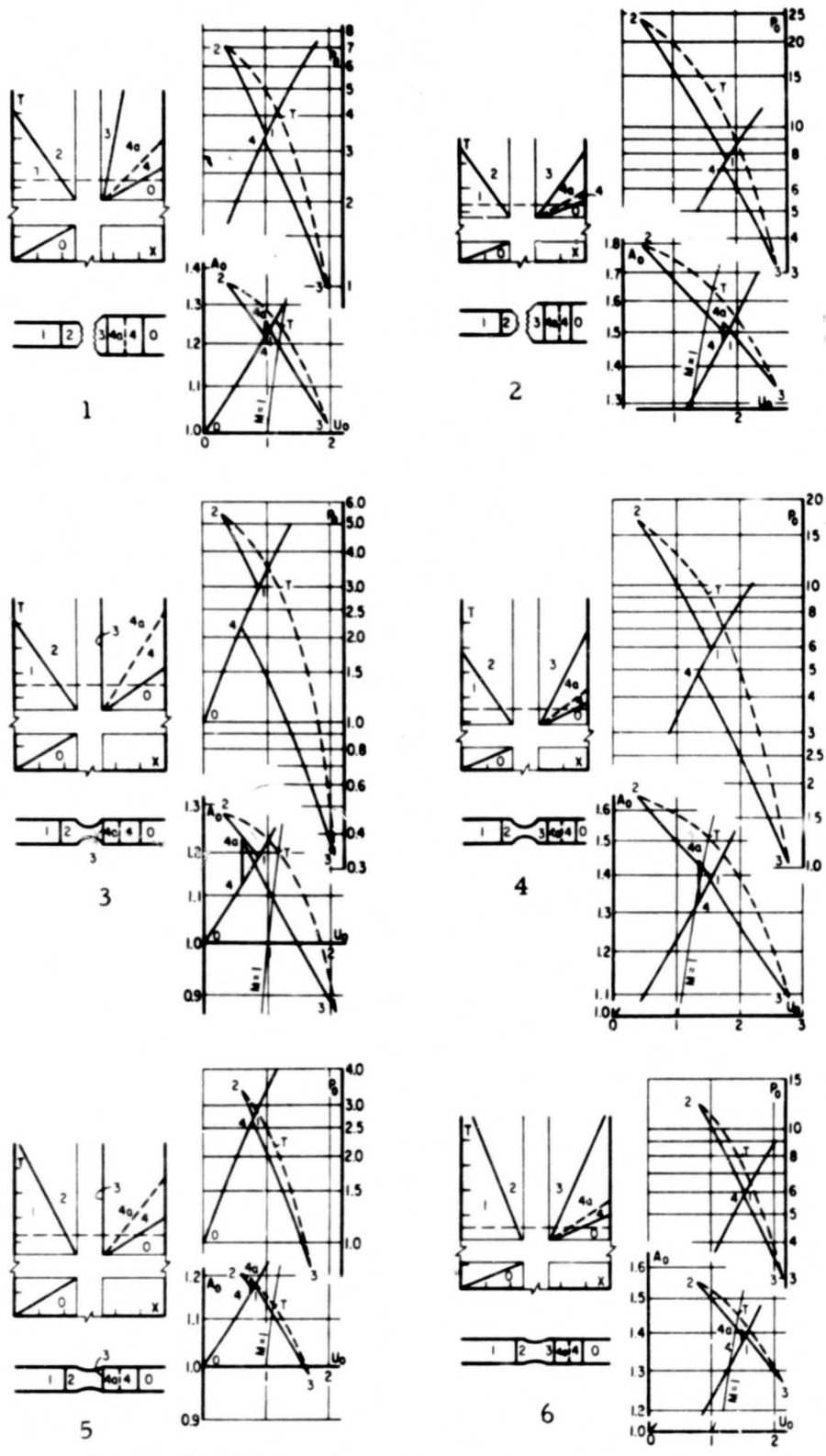

Fig. 26. Shock Interactions with Convergent-Divergent Nozzles

1. $M_i = 1.767$: $R_c = 0.444$: $R_d = 1.666$
2. $M_i = 2.581$: $R_c = 444.0$: $R_d = 1.666$
3. $M_i = 1.649$: $R_c = 0.38$: $R_d = 2.64$
4. $M_i = 2.30$: $R_c = 9.38$: $R_d = 2.64$
5. $M_i = 1.58$: $R_c = 0.75$: $R_d = 1.334$
6. $M_i = 2.30$: $R_c = 0.75$ $R_d = 1.334$

Such circumstances prevail in the regime to the left of both branches of Line I. To the right of this boundary the solution for shock interaction with a nozzle can be obtained by combining solutions for convergent and divergent sections. For this purpose one has to know only the compatible state at the throat that represents the outflow conditions for one and the inflow for the other. It turns out that such conditions are given by lines IV and III in Fig. 27. The required matching of the convergent part with the divergence is indicated there by thin guidelines. They connect corresponding points on the two sides of the $R = 1$ axis so that, having entered the diagram with a given value of M_i for the convergence, the corresponding value of M_i for the divergence is obtained by following the appropriate guideline up to Line I or III as illustrated in Fig. 27.

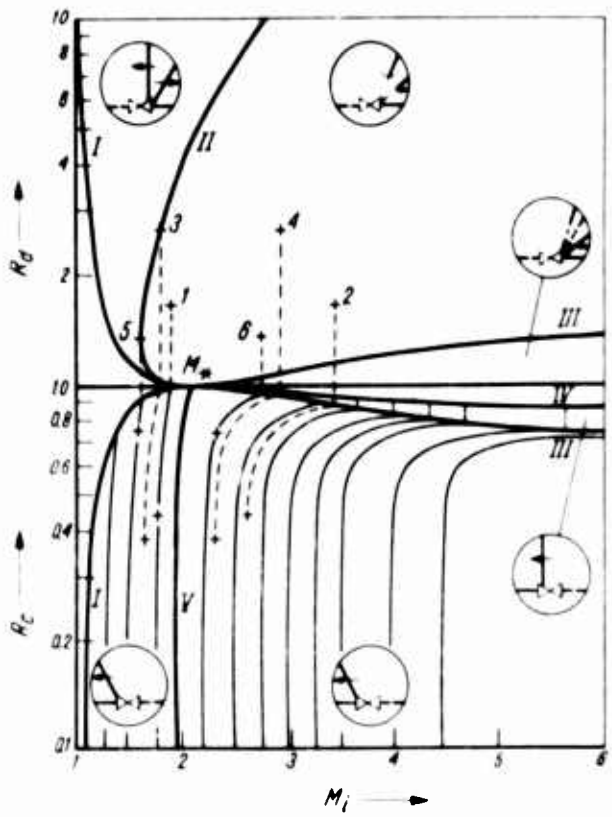

Fig. 27. Regimes od Solutions for Shock Interactions with Convergent-Divergent Nozzles in the Mach Number-Area Ratio Plane ($\gamma = 1.40$)

As previously, boundaries of the different regimes of solutions in the $M_i - R$ plane have been determined analytically and are described in Appendix 2.

Finally it should be noted that similar diagrams can be easily constructed for other values of γ by the use of the auxiliary plot of Fig. 24 in the same manner as it has been done for Fig. 25.

Incidentally, the case of a divergent-convergent duct has been left out of our considerations, since it does not lead to any interesting results. As contrasted to convergence, the divergence produces a change of state away from choking so that, for most initial conditions, the net results of shock interaction with such a duct is the same as that pro-

duced by a single area change. Any other case can be solved, of course, without any difficulty by the use of the vector polar method following the same procedure as that described here for the convergent-divergent nozzle.

5. Performance of Shock Tubes with Area Change at the Diaphragm Section

One of the well known techniques of increasing the performance of shock tubes is the use of an area change at the diaphragm section. This has been first proposed by Lukasiewicz (1950), while later Alpher and White (1958) presented an analytical method for the computation of the performance of such shock tubes.

Considered here first are cases involving a single divergence at the diaphragm section, then a single convergence, and finally a convergent-divergent nozzle. As before, our analysis leads to a specific delineation of regimes of solutions on a chart with, this time, the diaphragm pressure ratio and the area ratio as coordinates.

It appears that, by increasing the diaphragm pressure ratio in the case of a given divergence, one obtains first a transmitted shock with a reflected rarefaction, then a standing shock solution followed by a regime of swept-back shocks, and finally, a circumstance that somehow escaped the notice of others, of swept-back rarefactions. In the case of a single convergence there are only two regimes, one with transmitted shock, and the other with transmitted shock and a rarefaction anchored at the inlet to the convergence; both are associated with the usual rarefaction, characteristic of the shock tube problem, that propagates into the driver section. The effect of the addition of a convergence to precede the divergence, resulting in a convergent-divergent nozzle, is to displace the boundary curves on the diaphragm pressure-area ratio plane in the direction of smaller pressure ratios.

5.1. Effects of Single Area Changes

Cases 1 to 4 in Fig. 28 are representative of solutions obtained with the area divergence. The method of presentation is the same as before, i.e. each figure contains on the left the sketch of the physical X—T plane with the wave world-lines resulting in each case drawn to scale, on the right are the hodograph state diagrams with the pressure-velocity solution above and the velocity of sound-hodograph plane below. The substance in all cases of Fig. 28 is a perfect gas with $\gamma = 1.4$.

Case 1 corresponds to the diaphragm pressure ratio $P = 2.62$ and area ratio (low pressure to high pressure side) $R = 1.25$. It results in a transmitted shock followed by contact surface and a rarefaction propagating upstream — the typical wave pattern of a shock tube problem.

In Case 2 there appears a standing shock wave in the divergence, its existence is necessary in order to satisfy the compatibility conditions requiring the hodograph diagram in the P—U plane to be closed. The appearance of the standing shock is associated with the generation of a new state denoted by 1.2 so that the flow in the divergence is at first supersonic from state (3) to (2) where a change of state takes place across a shock from 2 to 1.2 followed by steady state, subsonic flow from 1.2 to 1.

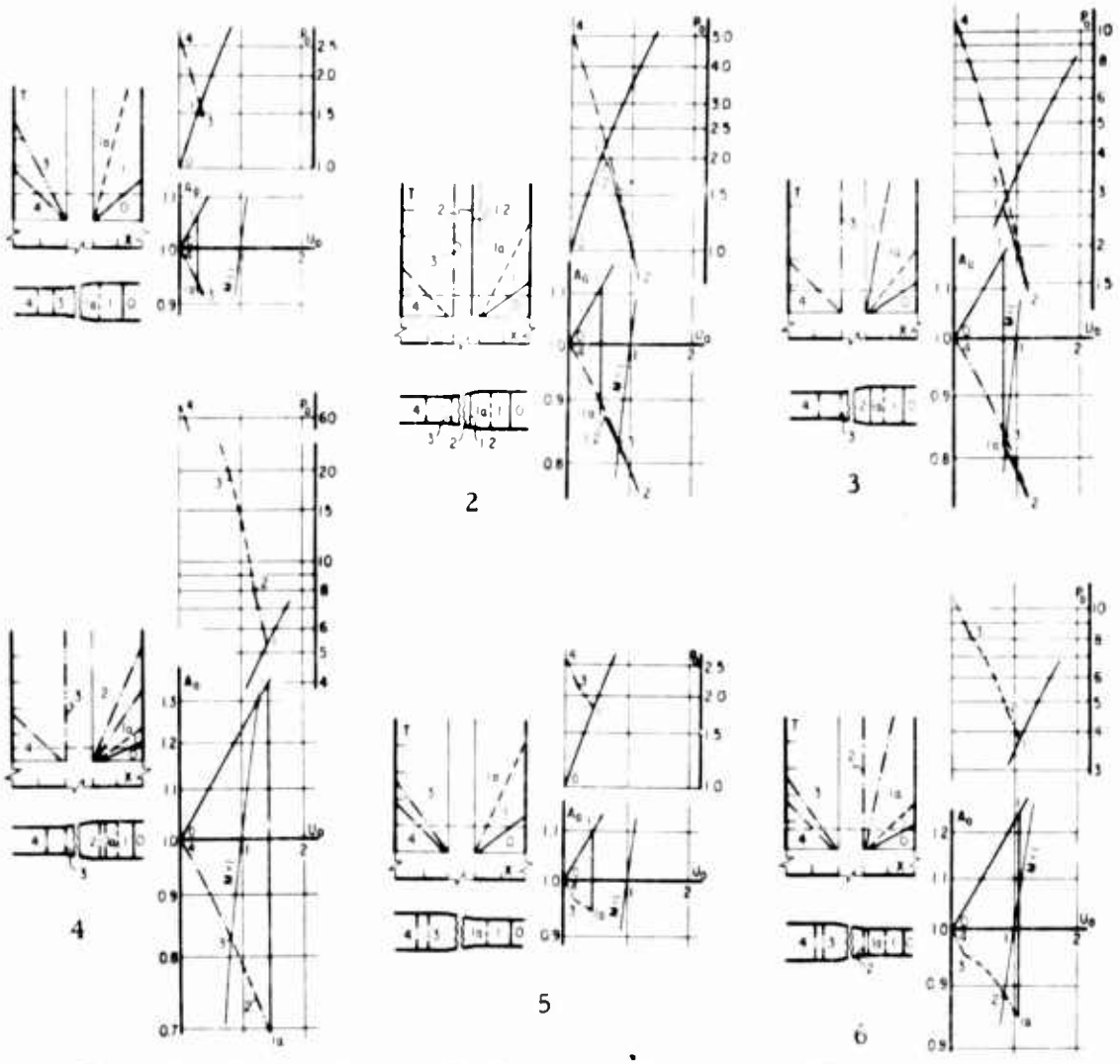

Fig. 28. Wave Systems Obtained with Single Area Changes at the Diaphragm Section
1. P_4 2.62: R 1.28 2. P_4 5.47: R 1.25 3. P_4 11.1: R 1.25
4. P_4 67.0: R 1.25 5. P_4 2.62: R 0.444 6. P_4 11.1: R 0.444

As the pressure ratio is increased further, the standing shock is pushed downstream of the nozzle so that in Case 3 it appears as a swept-back wave 2—1a.

For still higher diaphragm pressure ratios state 3 is shifted upwards in the $P-U$ plane while its velocity is fixed by the condition of $M = 1$ on the $A-U$ diagram. Since the change from state 3 to state 2 is specified by the area change, conditions are finally achieved that cause state 2 to be shifted to the left side of the incident shock polar on the $P-U$ plane. In order to satisfy the compatibility conditions, the change of state between the exit of the divergence and that immediately behind the transmitted shock involves then the action of a rarefaction rather than the swept-back shock. An example of such circumstances is presented by Case 4. The boundary line between the regime of solutions with the swept-back shock and that with the swept-back rarefaction, corresponds to the case of only a transmitted shock and a rarefaction propagating upstream with its trailing edge anchored at the inlet of the divergence.

Case 5 represents a typical result obtained with a convergence, practically identical with the elementary shock tube problem.

When the pressure ratio is increased while the area ratio remains unchanged, there appears a rarefaction propagating upstream on the low pressure side of the convergence and anchored at its outlet cross-section, as shown in Case 6.

The various solutions described in Fig. 28 are tabulated in Table 2 and are represented by the appropriate regimes in the diaphragm pressure-area ratio plane, Fig. 29, for the case of specific heat ratio $\gamma = 1.4$. Denoted there by numbers corresponding to the cases just described are points specifying their initial conditions. The analytical determination

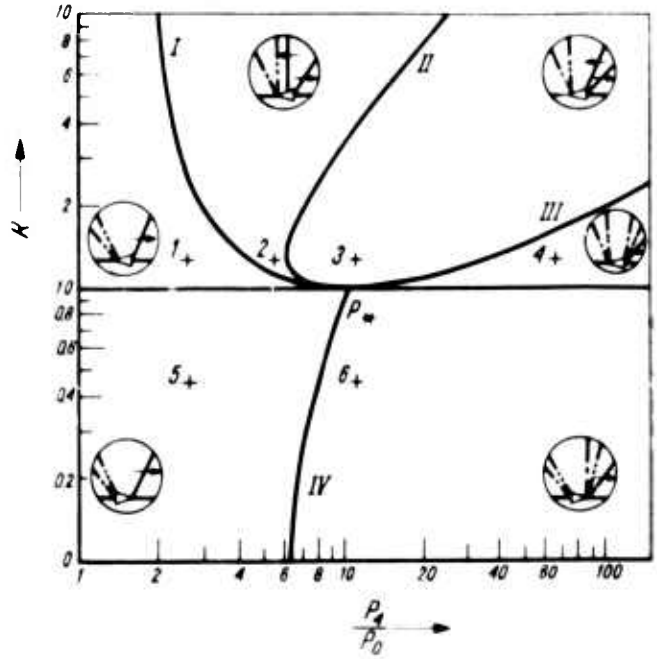

Fig. 29. Regimes of Solutions for a Single Area Change at the Diaphragm Section in the Pressure Ratio-Area Ratio Plane ($\gamma = 1.4$)

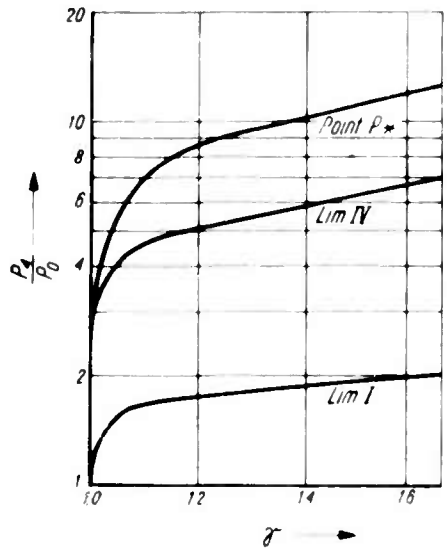

Fig. 30. Asymptotes of Boundaries in the Pressure Ratio-Area Ratio Plane as a Function of Specific Heat Ratio

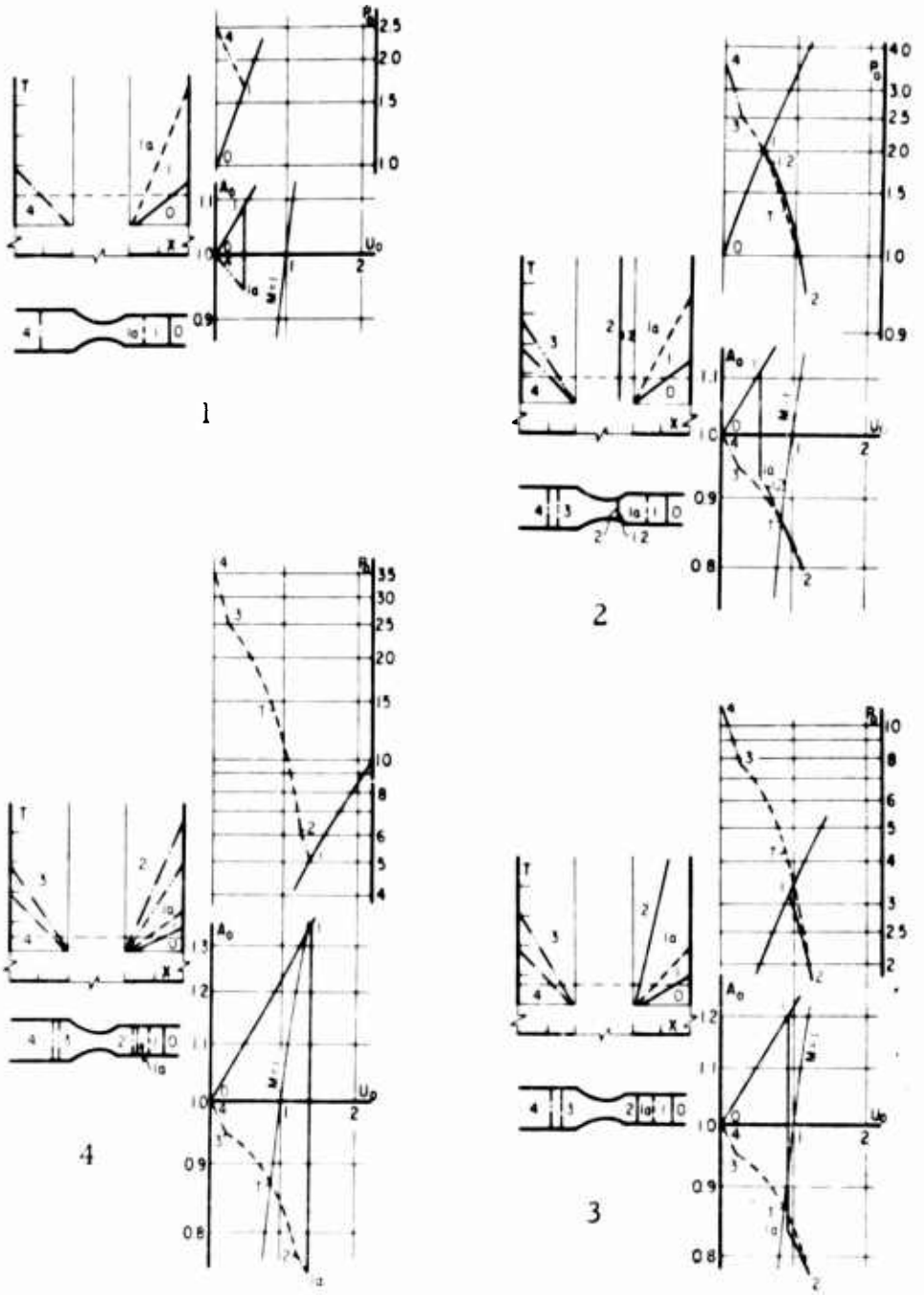

Fig. 31. Wave Systems Obtained with a Convergent-Divergent Nozzle
$R_c = 0.444$: $R_d = 1.25$, at the Diaphragm Section
1. $P_4 = 2.46$ 2. $P_4 = 3.67$ 3. $P_4 = 11.1$ 4. $P_4 = 36.6$

of the boundary lines of Fig. 29 is described in Appendix 3. The chart gives a comprehensive survey of all conditions that can be obtained with a single area change at the diaphragm section and covers specifically the range of area ratios from 0.1 to 10 and pressure ratios up to 150:1. Of particular interest is the regime characterized by point 4 which somehow escaped the notice of other investigators.

Fig. 30 gives values of asymptotes of the various boundary lines that appear in Fig. 29, as a function of the specific heats ratio, so that their effect could be estimated. Also included in Fig. 30 is the effect of the specific heat ratio on P_*, the point of intersection of all boundary lines in Fig. 29.

5.2. Effect of Convergent-Divergent Nozzle

Fig. 31 represents the various solutions obtained for the same convergent-divergent nozzle $R_c/R_d = 0.444/1.25$, with different diaphragm pressure ratios. Numerical results of these solutions are listed in Table 2.

Case 1 of $P = 2.46$ gives the same wave pattern as the elementary shock tube problem.

Increasing the diaphragm pressure ratio to 3.67 leads to Case 2 associated with the appearance of a standing shock in the divergence. Similarly as in Case 2 of Fig. 28, it should be noted that, as long as choking is not attained, i.e. the line of Mach number of unity in the $A-U$ plane is not reached, the solution is identical to that described previously. Now however the solution is determined completely by the overall area ratio (outlet to inlet) of the nozzle rather than by its shape. The convergent and divergent sections have to be considered separately the moment $M = 1$ is reached at the throat.

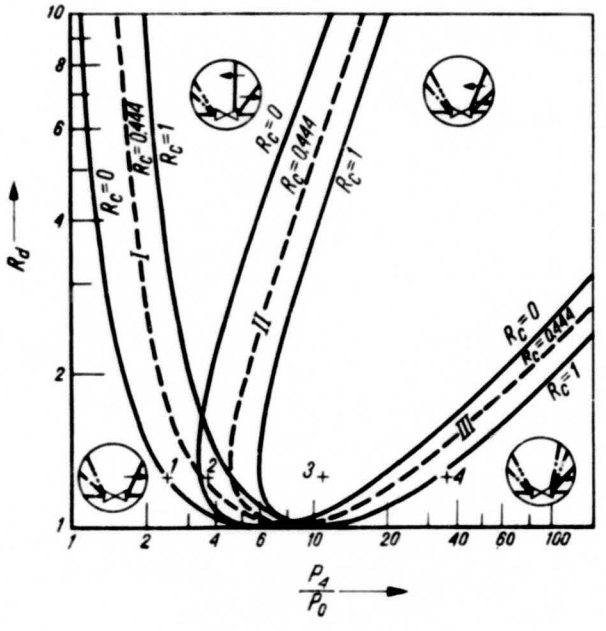

Fig. 32. Regimes of Solutions for Convergent-Divergent Nozzles at the Diaphragm Section in the Pressure Ratio-Area Ratio Plane ($\gamma = 1.4$)

Case 3 of Fig. 31 is equivalent to Case 3 of Fig. 28 resulting in a sweptback shock, while Case 4 has a similar wave pattern to Case 4 of Fig. 28, namely the swept-back rarefaction.

All the results obtainable with a convergent-divergent nozzle are summarized in Fig. 32 over the same range of the diaphragm pressures and area ratios as Fig. 29. Similar regimes are obtained here as before, the main effect of adding the convergence in shifting the

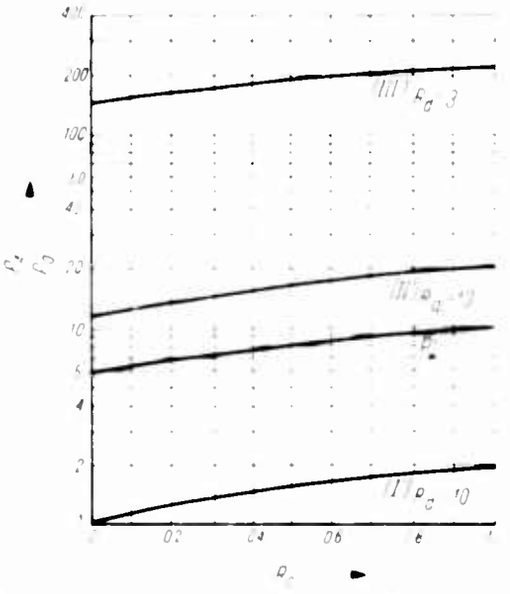

Fig. 33. Boundaries in the Pressure Ratio-Area Ratio Plane for R_d = 3 and 10, and the Critical Pressure Ratio, P_*, as a Function of R_c.

boundaries to the left, that is in the direction of smaller pressure ratios. This permits the attainment of the same wave pattern with lower initial pressure ratio by the use of a nozzle than in the case of a divergence alone.

In order to make the coverage of the effect of a nozzle at the diaphragm more comprehensive, the variation of the characteristic points of the boundary lines has been computed for the whole range of possible convergences R_c from 0 to 1, and the diaphragm pressure ratios P_4 from 1 to 400 as shown on Fig. 33. Since the shape of the lines remains practically the same, the determination of the boundaries for any given convergence in Fig. 32 is, with the help of Fig. 33, quite simple.

5.3. Case of Different Gases on the Two Sides of the Diaphragm

The use of the area change at the diaphragm section is often associated with that of different gases on its two sides. This has been indeed the case treated by Alpher and White (1958) who were concerned in particular with helium and hydrogen as drivers in combination with air, nitrogen and argon in the driven section. The problem then was to evaluate, for a given convergence, the pressure ratio that would drive a shock wave of a given strength.

In order to apply the vector polar method to such a problem, it is convenient to introduce an auxiliary diagram. Since, as demonstrated by the graphical solution of Fig. 34

... work back from a given state 1 by trial and error, the effort is considerably reduced if a single change of state from 1 to 2 is known *a priori*. This involves the knowledge of the change of state produced by a rarefaction combined with a steady flow across a duct with a given area change. Such a process is represented on the auxiliary graph, Fig. 35, which corresponds to a simple rarefaction fan followed by steady flow through a convergence $R_c = 0.444$, in the case of the same gases when $A_4 = 1$, and for the helium-argon combination, corresponding to $A_4 = 3.16$. The polars are obtained simply by adding vectorially the changes of state produced by a rarefaction fan followed by that for a given steady flow through the convergence.

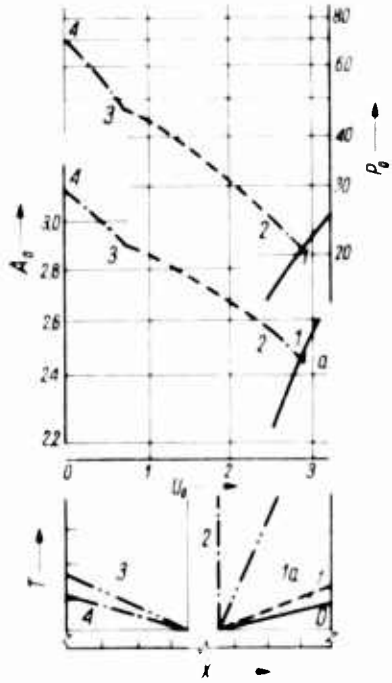

Fig. 34. Wave System Obtained with a Convergence at the Diaphragm Section Using Helium Driver and Argon as Driven Gas, $P_4 = 70.0$; $R_c = 0.444$

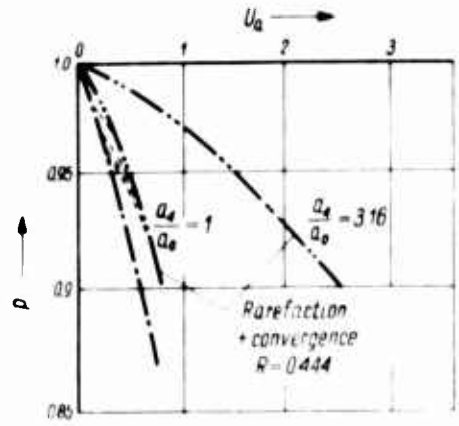

Fig. 35. Auxiliary Combination Polars for Rarefaction and Steady Flow throug Convergence with $R_c = 0.444$ ($\gamma = 5/3$)

A solution such as that of Fig. 34 for $P = 70$ and $R_c = 0.444$, is obtained with the use of the auxiliary graph quite easily on the $P - U$ plane. In this case the change of state from 4 to 2 is fixed. For a given position of state 1 on the initial shock polar, state 2 is determined by simple trial and error, so that state 4, at a fixed distance from it, would lie on the $U = 0$ axis. Numerical results of the solutions are listed in Table 2.

The agreement between the solutions obtained with the use of the vector polar method and those obtained by Alpher and White is indeed quite satisfactory, as demonstrated in Table 3.

6. Appendix I

Properties of Boundaries in the $M_i - R$ Plane, Fig. 23

6.1. Regime of Reflected Rarefaction

Line I separates the regime where the interaction produces a transmitted shock with a rarefaction fan propagating upstream and subsonic flow through the divergence from that where a standing shock appears inside the divergence. It is characterized by the condition of sonic inflow at the throat with subsonic isentropic flow through the divergent section. The relationship between R and M_i for this boundary, shown as Line I in Fig. 23, is determined from the following equations describing the state immediately behind the transmitted shock wave of Case 1, Fig. 21:

$$U_3 = \frac{(\gamma - 1)U_1 + 2A_1}{\gamma + 1} - \frac{1}{R}(M_{3a}R)^{-\frac{2}{\gamma+1}} \tag{35}$$

$$P_3 = P_1\left(\frac{\gamma - 1}{\gamma + 1}M_1 + 2\right)^{\frac{2\gamma}{\gamma-1}}(M_{3a}R)^{-\frac{2\gamma}{\gamma+1}} \tag{36}$$

The velocity ratio, $U_1 = u_1/a_0$, local velocity of sound ratio, $A_1 = a_1/a_0$ and pressure ratio, $P_1 = p_1/p_0$, are, in turn, related by the shock relations (12) and (13) while $U_3 = u_3/a_0$ and $P_3 = p_3/p_0$ are also related by equation (11). The Mach number of the flow immediately behind the divergence is related to the area ratio by the steady flow relation:

$$R = \frac{1}{M_{3a}}\left[\frac{2}{\gamma + 1}\left(1 + \frac{\gamma - 1}{2}M_{3a}^2\right)\right]^{\frac{\gamma+1}{2(\gamma-1)}} \tag{37}$$

which holds true when the flow at the inlet to the divergence is exactly sonic — the characteristic feature of Line I.

We have thus seven equations for the eight variables u_3/a_0, p_3/p_0, u_1/a_0, a_1/a_0, p_1/p_0, M_i, M_{3a} and R, which lead to a unique relation between M_i and R. For $R_I = \infty$ the equations can be reduced to a single relationship:

$$\left|(M_i^2 - 1)(\gamma - 1)^{\frac{1}{2}} - \left(M_i^2 + \frac{2}{\gamma - 1}\right)^{\frac{1}{2}}[2\gamma M_i^2 - (\gamma - 1)]^{\frac{1}{2}}\right|^2 = \frac{1}{2}(\gamma + 1)^{\frac{2\gamma-1}{\gamma}}\left(M_i^2 + \frac{2}{\gamma - 1}\right)[2\gamma M_i^2 - (\gamma - 1)] \tag{38}$$

which determines the value of the asymptote; e.g. for $\gamma = 1.40$ it yields $\lim_{R_1 \to \infty} M_i = 1.15$. Asymptotes for other values of γ are given in Table I.

The incident shock Mach number, M_*, at which all boundary lines intersect, is evaluated from the shock relations (11), (12) and (13) for the condition $M_1 = 1.0$, yielding:

$$M_i = M_* = \left[\frac{(7-\gamma) - (\gamma^2 - 2\gamma + 17)^{\frac{1}{2}}}{4(2-\gamma)}\right]^{\frac{1}{2}} \tag{39}$$

which, for $\gamma = 1.4$, results in $M_* = 2.069$. Critical Mach numbers for other values of γ are listed in Table I.

6.2. Regime of Standing Shock Solution

Line II in Fig. 23 is the upper bound for the regime of the standing shock solution, and represents the case of a shock stabilized at the end of the divergence. For higher values of M_i the flow velocity at the exit is too high to maintain there a stationary shock, and it is therefore swept downstream, as shown in Case 3 of Fig. 21.

The boundary is determined by the conditions behind the transmitted shock:

$$U_4 = \frac{\gamma - 1}{\gamma + 1}\left(U_1 + \frac{2}{\gamma - 1}A_1\right)\frac{M_3^2 + \dfrac{2}{\gamma - 1}}{M_3(M_3R)^{\frac{\gamma-1}{\gamma+1}}} \tag{40}$$

$$P_4 = \frac{2\gamma}{\gamma + 1}P_1\left[\frac{\gamma - 1}{\gamma + 1}\left(M_1 + \frac{2}{\gamma + 1}\right)\right]^{\frac{2\gamma}{\gamma-1}}\frac{M_3^2 - \dfrac{\gamma - 1}{2\gamma}}{(M_3R)^{\frac{2\gamma}{\gamma+1}}} \tag{41}$$

supplemented by the shock relations (11), (12) and (13) giving the particle velocity, sound speed and pressure behind the shock in terms of its Mach number. When the Mach number of the incident shock is lower than the critical (e.g. $M_i^* = 2.069$ for $\gamma = 1.4$), the flow into the divergence is sonic and the relation between the Mach number of the flow immediately behind the divergence and the area ratio is again given by eqn. (37).

For supercritical Mach numbers the incident shock produces supersonic flow with respect to the duct and the condition of $M = 1$ at the entrance is no longer valid. For this reason equation (37) is not applicable, and the rarefaction process included in the derivation of equations (40) and (41) is omitted, since there is no rarefaction wave propagating upstream. The new relations for U_4 and P_4 are then given by:

$$U_4 = \frac{2}{\gamma + 1}A_1\frac{\left(1 + \dfrac{\gamma - 1}{2}M_1^2\right)}{\dfrac{\gamma - 1}{\gamma + 1}M_1}\frac{(RM_3)^{\frac{\gamma-1}{\gamma+1}}}{M_3} \tag{42}$$

$$P_4 = \frac{2\gamma}{\gamma + 1}P_1\left(M_3^2 - \frac{\gamma - 1}{2\gamma}\right)\left(R\frac{M_3}{M_1}\right)^{-\frac{2\gamma}{\gamma+1}} \tag{43}$$

Line II goes to infinity in both R and M_i so that for an incident shock of any strength there is a divergence beyond which the interaction results in a standing wave.

6.3. Regime of Peculiarity of Shock Interaction with a Convergence

For small area ratios the flow behind a sufficiently strong incident shock remains supersonic across the convergence. For larger area ratios the same incident shock produces, on the other hand, a reflected wave with subsonic flow through the convergence and a choking state at the throat.

The upper bound for supersonic flow, Line III, in Fig. 23 corresponds to the case of a rarefaction anchored at the exit of convergence; the lower bound for the reflected shock solution, Line IV, in Fig. 23 is that of a standing shock at the entrance to the convergence. It turns out that the two boundaries overlap each other, so that in effect the $R - M_i$ plane is folded over, producing the regime of peculiarity, referred to in the text, where three solutions are possible at the same time.

The relationship for Line III is simply obtained by combining equation (11) with the equation for steady state choked flow:

$$\frac{1}{R} = \frac{1}{M_1}\left[\frac{2}{\gamma+1}\left(1 + \frac{\gamma-1}{2}M_1^2\right)\right]^{\frac{\gamma+1}{2(\gamma-1)}} \tag{44}$$

For Line IV the set of equations is modified in that the Mach number M_1, appearing in equation (44) instead of being determined by the flow behind the incident shock, is attained by a normal shock propagating into this state, as shown in Case 9, Fig. 22. The modification involves the use of M_2 in equation (44) which is related to M_1 by the normal shock relation:

$$M_2 = \sqrt{\frac{M_1^2 + \dfrac{2}{\gamma-1}}{\dfrac{2\gamma}{\gamma-1}M_1^2 - 1}} \tag{45}$$

The asymptotic values corresponding to the incident shock Mach number of infinity are given by:

$$\lim_{M_i\to\infty} R_{III} = (\gamma-1)^{-\frac{1}{2}}\left(\frac{\gamma}{2}\right)^{\frac{1}{\gamma-1}} \tag{46}$$

$$\lim_{M_i\to\infty} R_{IV} = (\gamma-1)^{\frac{1}{2}}\left[\frac{\gamma}{2}(3-\gamma)\right]^{\frac{1}{\gamma-1}} \tag{47}$$

For $\gamma = 1.40$ this results in $\lim_{M_i\to\infty} R_{III} = 0.648$ and $\lim_{M_i\to\infty} R_{IV} = 0.838$. Both asymptotes for different values of γ are listed in Table I.

6.4. Regime of Reflected Shock and Subsonic Flow through Convergence

Line V in Fig. 23 separates the regime where the interaction of a weak shock with an area convergence results in a wave system consisting of a transmitted shock, a reflected shock and fully subsonic flow through the convergence (Case 10, Fig. 22) from that where

choking occurs at the throat with an anchored rarefaction there (Case 9, Fig. 22). It is characterized by the condition of sonic flow at the throat section without the appearance of the rarefaction downstream of the convergence. The boundary is obtained again from equations describing the state behind the transmitted shock where, in this case, one has to take into account the change of state brought about by the reflected shock, so that now

$$U_3 = \left| U_1 \quad \frac{2}{\gamma + 1} \quad A_1 \quad \frac{M_r^2 \quad 1}{M_r} \right| \frac{1}{M_2} \left(\frac{M_2}{R} \right)^{\frac{\gamma-1}{\gamma+1}} \tag{48}$$

$$P_3 = P_1 \left[1 + \frac{2\gamma}{\gamma + 1} (M_r^2 \quad 1) \right] \left(\frac{M_2}{R} \right)^{\frac{2\gamma}{\gamma+1}} \tag{49}$$

The variables U_1, P_1, and A_1 are related to the Mach number of the incident shock wave, M_i, by equations (11), (12), and (13) while for sonic flow at the throat M_2 is related to R by equation (43). Combining equations (48) and (49) by means of equation (11) yields then one equation with three unknowns, M_i, M_r, and R. The additional relation required to plot line V is supplied by writing u_1/a_1 as:

$$\frac{u_1}{a_1} = M_2 \frac{a_2}{a_1} \quad \frac{u_2 \quad u_1}{a_1} \tag{50}$$

which, by again using the shock relations (11), (12), and (13), can be also expressed in terms of M_i, M_r, and R. The asymptotic value of the Mach number of the incident shock wave, M_i, which is attained for the area ratio of $R = 0$, is found by imposing the additional condition for the reflected shock from a closed end,

$$\frac{u_2}{a_2} \quad M_2 \quad 0$$

For the case of a perfect gas with $\gamma = 1.40$, the asymptotic value of $M_i = 1.719$. The values of $\lim_{R \to \infty} M_i$ for other values of γ are shown in Table I.

7. Appendix II

Properties of Boundaries in the M_i R Plane, Fig. 27

7.1. Regime of Subsonic Unchoked Flow

Choking at the throat of a convergent-divergent nozzle is of particular importance, in that it fixes the inlet condition for the divergent section. For each incident shock there is a certain area ratio of the convergence that produces choked flow without a reflected shock wave. Line I and V in Fig. 27 represent the locus of such conditions. Any problem to the left of these lines, i.e. when convergence does not lead to choking at the throat, may be treated as a single area disturbance with $R = R_c R_d$ representing the total area ratio. On the other hand in the regime to the right of Line V, there will result choking at the throat with a reflected shock, and the corresponding solution for the divergent section has to be found by the use of guide lines in Fig. 27.

The equation for Line V is derived by combining the shock equations (11), and (12) with the expression for the area ratio, R, corresponding to choked flow (44), yielding the following closed form relation between M_i and R_c:

$$\frac{1}{R_c^2} = \frac{\gamma(\gamma-1)}{2} f(M_i)\left[\frac{2}{\gamma+1}\left(1-\frac{1}{\gamma f(M_i)}\right)\right]^{\frac{\gamma+1}{\gamma-1}} \tag{51}$$

where

$$f(M_i) = \frac{\left(M_i^2 - \frac{\gamma-1}{2\gamma}\right)\left(M_i^2 - \frac{2}{\gamma-1}\right)}{(M_i^2-1)^2} \tag{52}$$

As R_c approaches zero this boundary approaches its asymptotic value of unity, i.e.:

$$\lim_{R_c \to 0} M_i = 1$$

The equation for Line I is obtained by noting that the flow through the nozzle is isentropic. Therefore the boundary Line I corresponds to the case of nozzles between tubes of equal cross-sectional area, i.e. $R = R_c R_d = 1$, and Line I is simply a reciprocal of Line V. Hence, from inspection of equation (51) its equation is:

$$R_d^2 = \frac{\gamma(\gamma-1)}{2} f(M_i)\left[\frac{2}{\gamma+1}\left(1-\frac{1}{\gamma f(M_i)}\right)\right]^{\frac{\gamma+1}{\gamma-1}} \tag{53}$$

and the asymptote is:

$$\lim_{R_d \to \infty} M_i = 1$$

7.2. Regime of Standing Shock Solution in the Divergence

Beyond Boundary Line I a standing shock is generated somewhere inside the divergence section of the nozzle. Line II serves the same purpose as Line II in Fig. 23, namely it represents the case when the standing shock created in the divergence is stabilized at its end. One can deduce the relation between R and M_i for Line II by noting that once the flow becomes choked at the entrance to the divergence, the flow through it is independent of the processes producing the choked condition. To each state along the $M = 1$ locus there corresponds a value of area ratio, R_d, that will produce a standing shock at the exit. In the case of single area disturbance described in Fig. 23 such state was determined by the change of state produced by the incident shock, M_i, followed by a reflected rarefaction wave. In the nozzle case it corresponds to a different incident shock M_i', followed by a steady flow process through the convergence. For the same flow velocity at the throat, i.e. $U_2' = U_2$ the two incident shock Mach numbers are related as follows:

$$A_1'\left(\frac{M_1'}{R_d}\right)^{\frac{\gamma-1}{\gamma+1}} = \frac{(\gamma-1)U_1 + 2A_1}{\gamma+1} \tag{54}$$

where, by substitution of equations (11), (12), and (53), the left hand side of the equation may be then expressed in terms of M_i' and the right hand side in terms of M_i. Using then

the information of Fig. 23 on the dependence of the area ratio for a single divergence on the incident shock Mach number, together with equation (54), one can plot Line II in Fig. 27.

For stronger incident shocks, i.e. $M_i > M_*$, the flow through the convergence becomes supersonic and the compatibility condition for the divergent section dominates the establishment of the entire flow process. The expression for Line II can be then deduced only from the shock relations (11) and (12), similarly as it was done for Line II in Fig. 23. The flow velocity and pressure ratio immediately behind the transmitted shock:

$$U_4 = A\left(\frac{M_1}{R_c}\right)^{\frac{\gamma-1}{\gamma+1}} (M_3 R_d)^{\frac{\gamma-1}{\gamma+1}} \tag{55}$$

$$P_4 = \frac{2\gamma}{\gamma+1} \cdot P_1 \left(\frac{M_1}{R_c}\right)^{\frac{2}{\gamma+1}} \frac{M_3^2 - \frac{\gamma-1}{2\gamma}}{(M_3 R_d)^{\frac{2\gamma}{\gamma+1}}} \tag{56}$$

are related by equation (11) while A_1, P_1, R_c, and M_1 can be expressed in terms of M_i by means of equations (11), (12), (13) and (44) and M_3 in terms of R_d by means of equation (37). Consequently, the above set of equations fixes the relationship between R_d and M_i for Line II.

In the limit when $M_i \to \infty$, the results of Fig. 23 still applies, i.e. for Line II.

$$\lim_{M_i \to \infty} R_{d_{II}} = \infty$$

7.3. Regime of Transmitted Rarefaction Propagation Upstream

In cases of small area divergences, stronger incident shocks produce weaker auxiliary shocks until finally the latter are annihilated forming a rarefaction fan instead. This transition of shock wave into rarefaction fan occurs along Line III. It is determined from the equation of supersonic choked flow through the convergence without reflection, followed by supersonic expansion through the divergence to the state behind the transmitted wave. Line III is then simply the isentropic supersonic extension of Line I and the relation between R_d and M_i is again given by equation (53), where M_i is now restricted to values greater than M_*. As the incident shock Mach number approaches infinity, R_d approaches its asymptotic value of

$$\lim_{M_i \to \infty} R_{d_{III}} = (\gamma - 1)^{\frac{1}{2}} \left(\frac{\gamma}{2}\right)^{-\frac{1}{\gamma-1}} \tag{57}$$

which for $\gamma = 1.40$ results in $\lim_{M_i \to \infty} R_{d_{III}} = 1.543$. The result for other values of γ are given in Table I.

7.4. Regimes of Solutions for Convergent Section

Strong incident shock waves impinging on nozzles with small convergences may produce standing shocks inside the convergent section in the same way as for a single convergence. The regime of such cases is delineated by Lines III and IV identical to those of

Fig. 23. The rest of the wave system depends on the divergent part of the nozzle. The regime between Lines IV and III represents the case of supersonic-unchoked flow at the throat. Similarly as the regime between Lines V and I, the resulting wave system is computed here again as if there was only a single area disturbance with an area ratio equal to the overall area ratio of the nozzle, i.e. $R = R_c R_d$.

8. Appendix III

Properties of Boundaries in the R – P Plane, Fig. 29

8.1. Regime of the Reflected Rarefaction Wave with Subsonic Flow through the Divergence

Line I separates the regime representing solutions with a transmitted shock, a rarefaction fan propagating upstream, and subsonic flow through the divergence, from that where a standing shock wave appears inside the divergence. It is characterized by the condition of sonic inflow at the throat with isentropic flow through the divergent section. The expression between R and P_1 for this boundary, shown as Line I in Fig. 29, is determined from the following equations describing the state immediately behind the transmitted shock wave of Case 1, Fig. 28:

$$U_1 = \frac{2}{\gamma + 1}\left(M_{1a} - \frac{1}{R}\right) \tag{58}$$

$$P_1 = P_4\left(\frac{\gamma + 1}{2} M_{1a} R\right)^{-\frac{2\gamma}{\gamma+1}} \tag{59}$$

The Mach number of the flow immediately downstream of the divergence is related to the area ratio by the steady flow expression (37) while equations (58) and (59) can be combined by means of the shock equation (11), leading thus to a unique relation between R and P_4.

The asymptotic value of P_1 corresponding to the area ratio of infinity is given by:

$$\lim_{R \to \infty} (P_1)_1 = \left(\frac{2}{\gamma + 1}\right)^{-\frac{2\gamma}{\gamma-1}}$$

which, for $\gamma = 1.4$, results in $\lim_{R \to \infty} (P_4)_1 = 1.89$. (For other values of γ see Table I).

The diaphragm pressure ratio, P_*, at which all boundary lines intersect, is determined by setting the area ratio and the Mach number of the flow behind the incident shock wave equal to 1.0. Equations (58) and (59) evaluated with the use of equation (11), lead to:

$$P_* = \left(\frac{\gamma + 1}{2}\right)^{\frac{2\gamma}{\gamma-1}} \left(\frac{2\gamma + 1 + \gamma\sqrt{5}}{\gamma + 1}\right) \tag{60}$$

which, for $\gamma = 1.4$, yields $P_* = 10.35$. (For other values of γ see Table I).

8.2. Regime of Standing Shock Solution

Line II in Fig. 29 is the upper bound for the regime of the standing shock solution and represents the case of a shock stabilized at the end of the divergence.

The boundary is determined from the conditions behind the transmitted shock wave of Case 3, Fig. 28:

$$U_1 = \frac{2}{(\gamma+1)^2}(M_2R)^{\frac{2}{\gamma+1}}\frac{1}{R}\left(\gamma - 1 + \frac{2}{M_2^2}\right) \tag{61}$$

$$P_1 = P_4\left(\frac{2}{\gamma+1}\right)^{\frac{2\gamma}{\gamma-1}}(M_2R)^{-\frac{2\gamma}{\gamma+1}}\left[1 - \frac{2\gamma}{\gamma+1}(M_2^2 - 1)\right] \tag{62}$$

which, together with the shock equation (11) and the steady flow relation (37) between the area ratio and the Mach number of the flow inside the exit plane of the divergence, yields the desired relation between R and P_4.

No asymptotic value exists for Line II since both R and P_4 go to infinity.

8.3. Regime of Transmitted Rarefaction Propagating Upstream

As the standing shock wave at the exit of the divergence is swept downstream, it decreases in strength and eventually becomes a downstream swept rarefaction wave. Line III is the locus of states representing the transition from compression to rarefaction. This case is identical to the wave system corresponding to Line I, with the exception that the flow behind the transmitted shock is now supersonic, so that equations (58) and (59) can be also used to determine Line III. Similar to Line II, no asymptotic value exists since again both R and P_4 go to infinity.

8.4. Regime of Anchored Rarefaction Downstream of Convergence

Line IV, Fig. 29, separates the regime representing solutions with a transmitted shock, a rarefaction fan propagating upstream, and subsonic flow through the convergence, from that where a rarefaction wave is anchored at the throat of the convergent section. It is characterized then by the condition of choked flow at the throat section.

The boundary is determined by the conditions behind the transmitted shock wave of Case 5, Fig. 28:

$$U_1 = \frac{\left(\frac{M_3}{R}\right)^{\frac{\gamma-1}{\gamma+1}}}{1 + \frac{\gamma-1}{2}M_3} \tag{63}$$

$$P_1 = P_4\left[\frac{\left(\frac{M_3}{R}\right)^{\frac{\gamma-1}{\gamma+1}}}{1 + \frac{\gamma-1}{2}M_3}\right]^{\frac{2\gamma}{\gamma-1}} \tag{64}$$

which, together with the shock wave equation (11) and the steady flow relation (44) between the area ratio and the Mach number of the flow into the convergence, are sufficient to relate uniquely R to P_4.

The asymptotic value of P_4 corresponding to $R = 0$ is given by:

$$\lim_{R\to 0}(P_4)_{IV} = \left(\frac{\gamma+1}{2}\right)^{\frac{\gamma}{\gamma-1}}\left[1+\frac{\gamma}{2}\left(1+\sqrt{\frac{9+\gamma}{1+\gamma}}\right)\right] \tag{65}$$

which, for $\gamma = 1.4$, yields $\lim_{R\to 0}(P_4)_{IV} = 5.92$. Asymptotic values of P_4 for other values of γ are listed in Table 1.

9. Appendix IV

Properties of Boundary Lines in the $R-P$ Plane, Fig. 32

The procedure for the derivation of equations for the boundary lines of Fig. 32 is essentially the same as that used for the case of a single area change at the diaphragm section, Fig. 29. However, for the present case the diaphragm pressure ratio, P_4, is a function of the two independent variables R_c and R_d which specify the geometry of the nozzle. It is necessary then to choose one of the area ratios as the independent variable and the other as a parameter for which a family of boundary lines could be determined. As apparent from Fig. 29, it is of greater interest to consider R_d as the variable and R_c as the parameter.

Boundary lines for a convergent-divergent nozzle have been computed for three values of R_c: 0, 0.444, and 1.0. Since, for each boundary line, sonic flow exists at the throat, the effect of the convergence is taken into account by the following relations describing the flow velocity and local pressure at the throat section:

$$\frac{u_T}{a_0} = \frac{\left(\frac{M_3}{R_c}\right)^{\frac{\gamma-1}{\gamma+1}}}{\left(\frac{\gamma-1}{2}\right)M_3+1} \tag{66}$$

$$\frac{p_T}{p_4} = \left(\frac{u_T}{a_0}\right)^{\frac{2\gamma}{\gamma-1}} \tag{67}$$

and the derivation of the boundary lines is then similar to that used for the single divergence. For sonic flow at the throat, the Mach number, M_3, of the flow into the convergence is related to the area ratio, R_c, by equation (44).

9.1. Regime of Subsonic Flow through the Divergence

Line 1 of Fig. 32 serves the same purpose as Line 1 in Fig. 29, in that it represents the case of sonic inflow at the throat with subsonic isentropic flow through the divergence, separating regimes of Case 1 from that of Case 2 of Fig. 31. In the present instance, however, the conditions behind the transmitted shock wave, related by the shock equation (11), are given by:

$$U_1 = U_T(M_{1a}R_d)^{\frac{2}{\gamma+1}}\frac{1}{R_d} \tag{68}$$

$$P_1 = P_4\frac{p_T}{p_4}(M_{1a}R_d)^{-\frac{2\gamma}{\gamma+1}} \tag{69}$$

where M_{1a}, the Mach number of the flow at the outlet of the divergence, is related to R_d by steady flow expression (37).

Since $(M_{1a}R_d) = \left(\frac{2}{\gamma+1}\right)^{\frac{\gamma+1}{2(\gamma-1)}}$ and $P_1 = 1$ as R_d goes to infinity, the expression for the asymptotic value of P_4 can be obtained directly from equation (69)

$$\lim_{R_d \to 0} P_4 = \frac{p_4}{p_T}\left(\frac{2}{\gamma+1}\right)^{\frac{\gamma}{\gamma-1}}$$

where p_4/p_T, determined by the area ratio of the convergence, is given by equations (66) and (67). For $R_c = 1.0$ the asymptotic expression reduces to that obtained for Line I, Fig. 29, namely

$$\lim_{R_d \to \infty} (P_4)_I = \left(\frac{2}{\gamma+1}\right)^{-\frac{\gamma}{\gamma-1}}$$

which, for $\gamma = 1.40$, yields $\lim_{R_d \to \infty} P_4 = 1.89$, while for $R_c = 0$,

$$\lim_{R_d \to \infty} P_4 = 1.0$$

9.2. Regime of Standing Shock Solution

Similarly as Line II in Fig. 29, Line II in Fig. 32 is the upper bound for the regime of the standing shock solution and represents the case of a shock stabilized at the outlet of the divergence. The boundary is determined from the shock equation (11) and the following expressions for conditions behind the transmitted shock wave of Case 3, Fig. 31:

$$U_1 = U_T R_d^{-\frac{\gamma-1}{\gamma+1}}\left[\left\{M_2^{\frac{2}{\gamma+1}}\left(1-\frac{2}{\gamma+1}\right)+\frac{2}{\gamma+1}M_2^{-\frac{2\gamma}{\gamma+1}}\right\}\right] \tag{70}$$

$$P_1 = P_4\frac{p_T}{p_4}(M_2R_d)^{\frac{2\gamma}{\gamma+1}}\left[1+\frac{2\gamma}{\gamma+1}(M_2^2-1)\right] \tag{71}$$

where M_2, the supersonic critical Mach number at the exit of the divergence, is related to R_d by equation (37).

No asymptotic value exists for Line II since, as in the case of the divergence at the diaphragm section, both R_d and P_4 go to infinity.

9.3. Regime of Transmitted Rarefaction Propagating Upstream

As the pressure ratio P_4 increases, the strength of the downstream swept shock wave of Case 3, Fig. 32, decreases and eventually becomes a downstream swept rarefaction wave. Line III, similar to Line III of Fig. 29, is then the locus of states representing the transition from compression to rarefaction. The wave system for Line III is therefore identical to that for Line I with the difference that now supersonic flow exists at the exit of the divergence. Equations (68) and (69) can be also used to determine Line III, except that the critical Mach number at the end of the divergent section is evaluated for supersonic flow.

Similarly as for Line II, no asymptotic value exists for Line III, since again both R_d and P_4 go to infinity.

Table 2

Solutions of Wave Interaction Problems

	State	M	P_0	A_0	U_0	V	W
Fig. 17	4	—	2.62	1	—	—	—
	1a	−1	1.584	0.933	0.33	−1	−1
		−1				−0.933	−0.60
	1	1.25	1.584	1.067	0.33	1.25	1.25
	2	−1.2	2.41	1.133	0	−1.28	−0.95
	3	+1	0.887	0.86	0	0.933	1.263
		+1				0.86	0.86
Fig. 18	1	1.6	2.75	1.173	0.8	1.6	1.6
	10	−0.14	0.61	2.47	1.8	−0.14	− 1.4
	2	−0.08	1.336	2.44	3.02	−0.21	0.59
	20	−1	1.15	2.41	3.28	−0.244	0.58
		−1				−0.241	0.87
	20a	1.37	1.15	2.62	3.28	3.38	5.18
Fig. 19	1	1.6	2.77	1.176	0.80	1.6	1.6
	2	1.6	7.7	1.39	1.77	1.88	2.68
	3a	−1	7.24	1.377	1.83	−1.39	0.38
		−1				−1.377	0.453
	3	2.54	7.24	1.49	1.83	2.54	2.54
Fig. 20	1	3.92	18	2	3.1	3.92	3.92
	2	+1	8.6	1.8	2.1	2.0	5.1
		+1				1.8	3.9
	3	−1.02	.05	1.81	2.04	−1.834	.27
	4	2.77	8.9	1.57	2.04	2.77	2.77
	2′	+1	3.56	1.585	1.04	2.0	5.1
		+1				1.585	2.625
	3′	—	—	—	—	—	—
	4′	1.78	3.56	1.246	1.04	1.78	1.78
	2″	+1	1.65	1.425	0.2	2.0	5.1
		+1				1.425	1.625
	3″	−1	1.506	1.405	0.32	−1.425	−1.225
		−1				−1.405	−1.085
	4″	1.2	1.506	1.067	0.32	1.2	1.2
Fig. 21—1	1	1.7	3.21	1.207	0.927	1.7	1.7
$R = 1.03$	2	−1	2.72	1.173	1.08	−1.207	−0.280
		−1				−1.173	−0.093
$M_i = 1.7$	3a	—	3.06	1.201	0.89	—	—
	3	1.668	3.06	1.201	0.89	1.668	1.668
	1	1.7	3.21	1.207	0.927	1.7	1.7
		−1				−1.207	−0.280
Fig. 21—2	2	−1	2.45	1.161	1.161	−1.161	0
$R = 1.08$	3	—	1.792	1.11	1.393	—	—
$M_i = 1.7$	3.4	−1.25	2.97	1.195	0.977	−1.388	0.005
	4a	—	3.06	1.203	0.907	—	—
	4	1.683	3.06	1.203	0.907	1.683	1.683

Table 2 (continued)

	State	M	P_0	A_0	U_0	V	W
	1	1.7	3.21	1.207	0.927	1.7	1.7
		−1				−1.207	−0.280
Fig. 21—3	2	−1	2.45	1.169	1.161	−1.161	0
$R = 1.25$	3	—	1.093	1.033	1.671	—	—
$M_i = 1.7$	4a	−1.578	2.99	1.214	0.87	−1.63	0.041
	4	1.65	2.99	1.197	0.87	1.65	1.65
	1	1.7	3.21	1.207	0,927	1.7	1.7
		−1				−1.207	−0.280
Fig. 21—4	2	−1	2.45	1.169	1.161	−1.161	0
$R = 4.45$	3	—	3.21	0.765	2.20	—	—
$M_i = 1.7$	3.4	−2.876	1.786	1.285	0.60	−2.20	0
	4a	—	1.878	1.244	0.47	—	—
	4	1.320	1.878	1.0975	0.47	1.320	1.320
	1	1.34	1.955	1.105	0.5	1.34	1.34
		−1				−1.105	−0.605
Fig. 21—5	2	−1	1.70	1.079	0.64	−1.079	−0.439
$R = 1.25$	3a	—	1.896	1.096	0.46	—	—
$M_i = 1.34$	3	1.33	1.896	1.096	0.46	1.33	1.33
	1	3.2	11.7	1.71	2.40	3.2	3.2
Fig. 21—6	3	—	6.83	1.583	2.80	—	—
$R = 1.25$	4a	−1.219	10.7	1.70	2.26	−1.93	0.87
$M_i = 3.2$	4	2.962	10.7	1.659	2.26	2.962	2.962
Fig. 22—7	1	3.2	11.7	1.71	2.40	3.2	3.2
$R = 0.95$	3	—	14.1	1.745	2.23	—	—
		−1				−1.745	0.485
$M_i = 3.2$	4a	−1	12.2	1.714	2.44	−1.714	0.726
	4	3.26	12.2	1.726	2.44	3.26	3.26
	1	3.2	11.7	1.71	2.4	3.2	3.2
Fig. 22—8	1.2	—	14.1	1.745	2.23	—	—
$R = 0.91$	2	−1.28	24.3	1.90	1.52	−2.23	0
$M_i = 3.2$	3	—	19.3	1.845	1.845	—	—
		−1				−1.845	0
	4a	−1	12.4	1.722	2.46	−1.722	0.738
	4	3.279	12.4	1.738	2.46	3.279	3.279
	1	3.2	11.7	1.71	2.40	3.20	3.20
Fig. 22—9	2	−1.48	28.5	1.962	1.20	−2.53	−0.13
$R = 0.84$	3	—	19.3	1.87	1.87	—	—
		−1				−1.87	0
$M_i = 3.2$	4a	−1	12.55	1.74	2.48	−1.74	−0.74
	4	3.30	12.55	1.746	2.48	3.30	3.30
Fig. 22—10	1	1.70	3.21	1.207	0.927	1.70	1.70
$R = 0.84$	2	−1.121	4.18	1.249	0.70	−1.354	−0.427
$M_i = 1.7$	3a	—	3.35	1.208	0.97	—	—
	3	1.737	3.35	1.221	0.97	1.737	1.737

Table 2 (continued)

	State	M	P_0	A_0	U_0	V	W
	1	1.767	3.44	1.228	1.00	1.767	1.767
Fig. 26—1	2	−1.373	7.1	1.356	0.36	−1.688	−0.688
$R_c = 0.44$	T	—	3.94	1.24	1.24	—	—
$R_d = 1.66$	3	—	0.97	1.017	1.96	—	—
$M_i = 1.767$	4a	−1.754	3.32	1.258	0.96	−1.785	0.175
	4	1.729	3.32	1.215	0.96	1.729	1.729
	1	2.581	7.60	1.489	1.83	2.581	2.581
Fig. 26.2	2	−1.681	23.9	1.79	0.50	−2.50	−0.67
$R_c = 0.44$	T	—	13.3	1.635	1.63	—	—
$R_d = 1.66$	3	—	3.285	1.339	2.63	—	—
$M_i = 2.58$	4a	−1.431	7.3	1.53	1.78	−1.915	0.715
	4	2.530	7.3	1.47	1.78	2.53	2.53
	1	1.649	3.00	1.192	0.868	1.649	1.649
Fig. 26—3	2	−1.304	5.48	1.304	0.30	−1.56	−0.692
$R_c = 0.38$	T	—	2.98	1.20	1.20	—	—
$R_d = 2.64$	3	—	0.331	0.87	2.07	—	—
$M_i = 1.649$	4a	−2.419	2.18	1.231	0.60	−2.1	−0.03
	4	1.418	2.18	1.125	0.60	1.418	1.418
	1	2.30	6.00	1.395	1.554	2.30	2.30
Fig. 26—4	2	−1.610	17.1	1.642	0.37	−2.241	−0.687
$R_c = 0.38$	T	—	9.3	1.506	1.506	—	—
$R_d = 2.64$	3	—	1.02	1.094	2.78	—	—
$M_i = 2.30$	4a	−2.063	4.9	1.445	1.34	−2.26	0.52
	4	2.084	4.9	1.325	1.34	2.084	2.084
	1	1.58	2.745	1.172	0.789	1.58	1.58
Fig. 26—5	2	−1.105	3.46	1.209	0.59	−1.295	−0.50
$R_c = 0.75$	T	—	2.18	1.131	1.12	—	—
$R_d = 1.334$	3	—	0.827	0.986	1.70	—	—
$M_i = 1.58$	4a	−1.716	2.66	1.20	0.77	−1.695	0.005
	4	1.557	2.66	1.166	0.77	1.557	1.557
	1	2.30	6.00	1.395	1.554	2.3	2.3
Fig. 26—6	2	−1.393	12.6	1.555	0.78	−1.945	−0.391
$R_c = 0.75$	T	—	7.91	1.454	1.44	—	—
$R_d = 1.334$	3	—	3.00	1.267	2.14	—	—
$M_i = 2.3$	4a	−1.348	5.86	1.411	1.52	−1.708	0.432
	4	2.273	5.86	1.375	1.52	2.273	2.273
Fig. 28—1	4	—	2.62	—	—	—	—
		−1				−1.0	−1.0
$R = 1.25$	3	−1	1.448	0.917	0.41	−0.917	−0.507
$P = 2.62$	1a	—	1.537	0.926	0.30	—	—
	1	1.208	1.537	1.06	0.30	1.208	1.208

Table 2 (continued)

	State	M	P_0	A_0	U_0	V	W
	4	—	5.46	—	—	—	—
						−1.0	−1.0
Fig. 28—2	3	—	1.537	0.8	0.83	−0.83	0
R = 1.25	2	—	0.772	0.75	1.14	—	—
P = 5.47	1.2	−1.52	1.952	0.87	0.603	−1.14	0
	1a	—	2.042	0.88	0.539	—	—
	1	1.373	2.042	1.113	0.539	1.373	1.373
	4	—	11.1	—	—	—	—
		−1				−1.0	−1.0
Fig. 28—3	3	−1	3.125	0.83	0.83	−0.83	0
R = 1.25	2	—	1.377	0.741	1.196	—	—
P = 11.1	1a	−1.353	2.72	0.823	0.78	−1.00	0.196
	1	−1.576	2.72	1.173	0.78	1.576	1.576
	4	—	67.0	—	—	—	—
		−1				−1.0	−1.0
Fig. 28—4	3	−1	18.7	0.83	0.83	−0.83	0
R = 1.25	2	—	8.25	0.741	1.196	—	—
		−1				−0.741	0.455
P = 67	1a	−1	5.31	0.693	1.42	−0.693	0.727
	1	2.166	5.31	1.352	1.42	2.166	2.166
	4	—	2.62	—	—	—	—
		−1				−1.0	−1.0
Fig. 28—5	3	−1	2.115	0.96	0.20	−0.96	−0.76
R = 0.444	1a	—	1.822	0.943	0.46	—	—
P = 2.62	1	1.312	1.822	1.096	0.46	1.312	1.312
	4	—	11.1	—	—	—	—
		−1				−1.0	−1.0
Fig. 28—6	3	−1	8.4	0.951	0.25	−0.95	−0.70
R = 0.444	2	—	4.71	0.883	0.883	—	—
		−1				−0.883	0
P = 11.1	1a	−1	3.74	0.848	1.08	−0.848	0.232
	1	1.83	3.74	1.252	1.08	1.83	1.83
Fig. 31—1	4	—	2.46	—	—	—	—
R_c = 0.444	1a	−1	1.70	0.944	0.40	—	−1
R_d = 1.25	1	1.265	1.70	0.925	0.40	1.265	1.265
P = 2.46							
	4	—	3.67	—	—	—	—
		−1				−1	−1
Fig. 31—2	3	−1	2.51	0.947	0.24	−0.947	−0.707
R_c = 0.444		—	1.405	0.87	0.807	—	—
R_d = 1.25	2	—	0.764	0.795	1.16	—	—
P = 3.67	1.2	−1.46	1.804	0.914	0.63	−1.16	0
	1a	—	2.075	0.932	0.55	—	—
	1	−1.38	2.075	1.116	0.55	1.38	1.38

Table 2 (continued)

	State	M	P_0	A_c	U_0	V	W
	4	—	11	—	—	—	—
		−1				−1	−1
Fig. 31—3	3	−1	7.7	0.947	0.24	−0.947	−0.707
R_c = —0.444		—	4.22	0.87	0.807	—	—
R_d = 1.25	2	—	1.86	0.774	1.24	—	—
P = 11.1	1a	−1.289	3.22	0.838	0.93	−0.995	0.245
	1	1.704	3.22	0.83	0.93	1.704	1.704
	4	—	36.7	—	—	—	—
		−1				−1.0	−1.0
Fig. 31—4	3	−1	25.00	0.947	0.24	0.947	−0.707
R_c 0.444		—	14.00	0.87	0.807	—	—
R_d = 1.25	2	—	6.18	0.774	1.24	—	—
		−1				−0.774	0.466
P = 36.6	1a	−1	5.10	0.748	1.37	−0.748	0.622
	1	2.124	5.10	0.75	1.37	2.124	2.124
	4	—	70.0	3.16	—	—	—
		−1				−3.16	−3.16
Fig. 34	3	−1	47.00	2.90	0.72	−2.90	−2.18
R = 0.444	2	—	24.50	2.55	2.55	—	—
		−1				−2.55	0
P = 70	1a	−1	20.5	2.44	2.88	−2.44	0.44
	1	4.075	20.5	2.47	2.88	4.075	4.075

Table 3

Solutions Obtained by Means of the Vector Polar Method in Comparison with Experimental and Analytical Results Recorded in the Literature

Reference	P_1	P_2/P_1			P_4		
		Literature		Vector Polar	Literature		Vector Polar
		Expr.	Analyt.		Exper	Analyt.	
Franks	3.0	1.96	1.9	1.84	2.3	2.4	2.18
	6.0	2.9	2.9	2.86	4.6	4.9	4.9
	9.0	3.45	3.6	3.63	6.5	7.4	7.5
Dosanjh	2.75 (M_1 = 1.58)	1.28	—	1.258	2.61	—	2.66
	6.0 (M_1 = 2.3)	2.18	—	2.095	5.43	—	5.86
Alpher and White	8	—	—	—	—	14.05	14.2
	10	—	—	—	—	20.15	20.0
	20	—	—	—	—	70	70

Praca wpłynęła do redakcji w grudniu 1963 r.

BIBLIOGRAPHY

1. R. A. Alpher and D. R. White, 1958, "Flow in Shock Tube With Area Change at the Diaphragm Section", J. Fluid Mech., Vol. 3, pp. 457—470.
2. J. Aschenbrenner, 1937, "Nichtstationäre Gasströmungen in Leitungen mit veränderlichem Querschnitt", Forsch. Geb. Ing. Wes., Vol 8, pp. 121—126; and "Der Einfluss der Gasträgheit auf den Liefergrad", ibid., pp. 285—294.
3. F. K. Bannister, and G. F. Mucklow, 1948, "Wave Action Following Sudden Release of Compressed Air Gas From a Cylinder", Proc. I. Mech. E., Vol. 159, p. 269.
4. G. A. Bird, 1959, "The Effect of Wall Shape on the Degree of Reinforcement of a Shock Wave Moving into a Convergent Nozzle", J. Fluid Mech., Vol. 5, pp. 60—66.
5. W. B. Brower, Jr., 1961, "An Investigation of the Flow Due to Shock Impingement on a Construction" TR AE 6107 (Rensselaer Polytechnic Institute, Troy, New York).
6. S. Ciolkowski, 1961, "Shock Impingement on a Construction" RE — 150 (Grumman Aircraft Eng. Co., New York).
7. R. Courant and K. O. Friedrichs, 1948, "Supersonic Flow and Shock Waves" (Interscience Publishers, Inc., New York).
8. D. S. Dosanjh, 1955, "Interaction of Grid With Traveling Shock Waves", J. of Aero. Sci., Vol. 22, pp. 797—799.
9. W. B. Fallis, G. W. Johnston, J. D. Lee, N. B. Tucker and J. H. T. Wade, 1953, "Design and Calibration at the Institute of Aerophysics 16″×16″ Supersonic Wind Tunnel", UTIA Rept. 15 (Institute of Aerophysics, Toronto).
10. J. V. Foa, 1960, "Elements of Flight Propulsion" (John Wiley and Sons, Inc., New York).
11. W. J. Franks, 1957, "Interaction of a Shock Wave With a Wire Screen", UTIA Rept 13 (University of Toronto, Canada).
12. I. I. Glass, and J. G. Hall, 1958, "Shock Tubes. I. Theory and Performance of Simple Shock Tubes. II. Production of Strong Shock Waves; Shock Tube Applications, Design and Instrumentation" (UTIA Review, 12, Toronto).
13. J. Hadamard, 1903, "Leçons sur la Propagation des Ondes et les Equations de l'Hydrodynamique" (Chelsea Publishing Co., New York).
14. P. Haller, de, 1945, "Über eine Graphische Methode in der Gasdynamik", Technische Rundschau Sulzer, Vol. 1, pp. 6—24.
15. H. Hugoniot, 1887, "Propagation du Mouvement dans le Corps", J. de l'Ecole Polytechnique, Paris, No. 57e, p.3, No. 58e, pp. 1—125.
16. E. Jenny, 1949, "Berechnungen und Modellversuche über Druckwellen Grosser Amplituden in Auspuffleitungen" (E. T. H. Promotionsarbeit, Ameba-Druck, Basel).
17. P. Kijkowski, 1959, "Praktyczne Sposoby Wyznaczania Parametrów Przepływu Gazu Ściśliwego w Przewodach" Technika Lotnicza, Część I, 113—122, Część II, 144—150.
18. J. Łukasiewicz, 1950, "Flow in a Shock Tube of Nun-Uniform Cross-Section" (MT 11, National Research Council of Canada, Ottawa).
19. R. Mises, von, 1958, "Mathematical Theory of Compressible Fluid Flow" (Academic Press, Inc., New York).
20. G. F. Mucklow, and A. J. Wilson, 1955, "Wave-Action in Gases: The Attenuation and Reflection of Compression Waves Propagated in Pipes", Proc. I. Mech. E., Vol. 169, pp. 69—82.
21. J. von Neumann, 1943, „Progress Report on the Theory of Shock Waves, National Defence Research Committee" (OSRD Report No. 1140).
22. A. K. Oppenheim, and R. A. Stern, 1958, "On the Development of Gaseous Detonation — Analysis of Wave Phenomena", 7th Symposium (Int'l) on Combustion (Butterworths, London) pp. 837—850.
23. A. K. Oppenheim, R. A. Stern, and P. A. Urtiew, 1960, "On the Development of Detonation With Pre-Ignition", Combustion and Flame, Vol. 4, pp. 335—341.
24. A. K. Oppenheim, P. A. Urtiew, and R. A. Stern, 1959, "Peculiarity of Shock Impingement on Area Convergence", Phys. Fluids, Vol. 2, pp. 427—431.

25. K. Oswatitsch, 1956, "Gas Dynamics" (Academic Press Inc., New York).
26. H. Pfriem, 1941, "Die Ebene Ungedämpfte Druckwelle Grosser Schwingungsweite", Forsch Geb. Ing. Wes., Vol. 12, pp. 51—64.
27. B. Riemann, 1859, "Uber die Fortpflanzung ebener Luftwellen von endicher Schwingungsweite", Abhandlungen der Mathematischen Classe der Königlichen Gesellschaft der Wissenschaften zu Göttingen (Göttingen, Germany) Vol. 8, pp. 43—65.
28. G. Rudinger, 1855, "Wave Diagrams for Non-Steady Flow in Ducts" (D. Van Nostrand Co., Inc., New York).
29. G. Rudinger, 1960, „On the Uniqueness of Solutions for Passage of Shock Waves Through Ducts of Variable Cross-Section", Phys. Fluids, Vol. 3, p. 449.
30 R. Sauer, 1942, "Characteristikenverfahren für die Eindimensionale Instationäre Gasströmung", Ingenieur Archiv, Vol. 13, p. 79—89.
31. F. Schultz-Grunow, 1944, "Zur Behandlung Nichtstationärer Verdichtungsstosse und Detonationswellen", Z. angew. Math. Mech., Vol. 24, p. 284—288.
32. K. P. Stanyukovich, 1960, "Unsteady Motion of Continuous Media", English translation edited by Maurice Holt, (Pergamon Press, London) 740 pp.
33. F. J. Wallace, and R. W. S. Mitchell, 1952, "Wave Action Following the Sudden Release of Air Through an Engine Port System", Proc. I. Mech. E., Vol. 1B, pp. 343—363.
34. J. K. Wright, 1961, "Shock Tubes" (John Wiley and Sons, Inc., New York).

Wektorowo-biegunowa metoda oceny procesów oddziaływania fal

Streszczenie

Praca poświęcona jest metodom graficznym rozwiązywania zagadnień związanych z rozchodzeniem się fal i ich wzajemnym oddziaływaniem. Metody te pozwalają przeanalizować wiele zagadnień związanych z powstawaniem i rozchodzeniem się fal, takich jak fale deflagracyjne, lub fale rozrzedzeniowe, zjawiskami związanymi z nagłą zmianą przekroju itp.

Zaletą metod podanych w pracy jest to, że pozwalają one w stosunkowo prosty sposób przeprowadzić dyskusję zjawisk, często znanych, a nawet niekiedy rozwiązanych analitycznie, i wykazać pewne nowe właściwości, trudne do otrzymania na drodze analitycznej.

Векторно-полярный метод вычисления процесса воздействия волн

краткое содержание

Работа посвящена графическим методам решения вопросов, связанных с распространением волн и их взаимодействием.

Эти методы позволяют проанализировать много вопросов, связанных с возникновением и распространением волн таких как дефлаграционные и волны разрежения, с явлениями связанными с внезапным изменением сечения и т.п.

Достоинством приведенных методов является тот факт, что они дают возможность продискутировать сравнительно простым способом явления часто известные, а даже иногда аналитически решенные, и показать некоторые новые свойства, трудные для получения аналитическим путем.

DOCUMENT CONTROL DATA – R&D

(Security classification of title, body of abstract and indexing annotation must be entered when the overall report is classified)

1. ORIGINATING ACTIVITY *(Corporate author)*
University of California
Berkeley, California

2A. REPORT SECURITY CLASSIFICATION
☒ Unclassified
☐ Other — Specify

2B. GROUP

3. REPORT TITLE

VECTOR POLAR METHOD FOR THE EVALUATION OF WAVE INTERACTION PROCESSES

4. DESCRIPTIVE NOTES *(Type of report and inclusive dates)*

☐ Scientific Report ☐ Final Report ☒ Journal Article ☐ Proceedings ☐ Book

5. AUTHOR(S) *(Last name, first name, initial)*

Oppenheim, A. K. (PI); Urtiew, P. A.; and Laderman, A. J.

6. REPORT DATE AS PRINTED
1964

7A. TOTAL NO. OF PAGES
55

7B. NO. OF REFS
34

8A. CONTRACT OR GRANT NO
AF-AFOSR 129-64

B. PROJECT NO
9711-01

C. 61445014

D.

9A. ORIGINATOR'S REPORT NUMBER(S) *(If given)*

9B. OTHER REPORT NO.(S) *(Any other numbers that may be assigned this report)*
AFOSR **65-1479**
AD

10. AVAILABILITY/LIMITATION NOTICES

☑ Available from DDC
☐ Available from CFSTI
☐ Available from Source
☐ Available Commercially

11. SUPPLEMENTARY NOTES *(Citation)*
Arch Budowy Maszyn V11 PP441-495 1964

12. SPONSORING MILITARY ACTIVITY
AF Office of Scientific Research SREP
Office of Aerospace Research
Washington, D. C. 20333

13. ABSTRACT
Vector polar method is a graphical technique for the solution of wave interaction problems that are concerned with the overall results rather than with the progress of the process, The method is based on the use of wave polars. If the ratio of pressures or sound speeds is represented on a logarithmic scale, usually as the ordinate, while the abscissa represents the change in particle velocity across the wave in a linear scale, then such a generalized hodograph plane has the property of a vector field. By simple vector addition, some quite complex wave interaction processes can then be rapidly evaluated. The utility of the method is illustrated by a variety of shock-tube problems involving interactions between shocks, deflagrations, rarefaction waves, contact discontinuities and area change. Although the analysis of most of such problems is known, the application of the vector polar method led to the discovery of some interesting regimes of solutions that would be difficult to discern by the more laborious conventional techniques. (U)